2-1-2012

Predicting adhesive failure initiation of an epoxy bond for electronic packaging survivability

Brenton Adam Elisberg

Brenton Elisberg

Candidate

Mechanical Engineering

Department

This thesis is approved, and it is acceptable in quality and form for publication:

Approved by the Thesis Committee:

Tariq Khraishi , Chairperson

Yu-Lin Shen

Robert Chambers

PREDICTING ADHESIVE FAILURE INITIATION OF AN EPOXY UNDERFILL FOR ELECTRONIC PACKAGING SURVIVABILITY

by

BRENTON ELISBERG

B.S., MECHANICAL ENGINEERING, UNIVERSITY OF NEW MEXICO 2009

THESIS

Submitted in Partial Fulfillment of the
Requirements for Degree for

Master of Science
Mechanical Engineering

The University of New Mexico
Albuquerque, New Mexico

December, 2011

ACKNOWLEDGEMENTS

I would like to express my deepest appreciation to Robert Chambers for his many years of mentorship. His instruction during my internship at Sandia National Laboratories and guidance during the course of this thesis has been most important to my success in school and my future as a mechanical engineer.

I would like to thank Scott Spangler, Jamie Kropka, Matthew Neidigk, Kevin Austin, and Ernest Gonzales for their assistance and advice during this thesis over the past year. Their knowledge has greatly improved my understanding of experimentalist techniques, laboratory conduct, and data analysis.

Finally I would like to thank my advisor, Tariq Khraishi, for providing his useful perspective and guidance during the course of my thesis as well as Yu-Lin Shen for his participation on my thesis committee.

Experiments and computational analysis for this thesis was performed at Sandia National Laboratories in Albuquerque, NM. The support and cooperation of Sandia Labs is acknowledged for the success of my thesis project.

Sandia National Laboratories is a multi-program laboratory managed and operated by Sandia Corporation, a wholly owned subsidiary of Lockheed Martin Corporation, for the U.S. Department of Energy's National Nuclear Security Administration under contract DE-AC04-94AL85000.

PREDICTING ADHESIVE FAILURE INITIATION OF AN EPOXY UNDERFILL FOR ELECTRONIC PACKAGING SURVIVABILITY

by

BRENTON ELISBERG

B.S., MECHANICAL ENGINEERING, UNIVERSITY OF NEW MEXICO 2009

M.S., MECHANICAL ENGINEERING

ABSTRACT

Epoxy underfills can be implemented in electronic packaging to enhance solder joint reliability of surface mounted components. However, it is important for an engineer to have a failure criterion that can be used for failure predictions and redesign of electronic assemblies. Data from epoxy bond failure in mock electronic part assemblies were correlated to finite element analyses to predict adhesive failure initiation. Experiments were performed to determine failure loads for various loading locations and nonlinear viscoelastic analyses were performed for the same loading locations to determine a maximum principal strain failure parameter. Predictions showed that a maximum principal strain failure parameter defined from one test could be used as an indicator of adhesive failure of an epoxy bond undergoing other modes of loading. Failure initiation predictions matched experimental data using a maximum principal strain failure parameter for an epoxy bond undergoing mixed modes of loading for both unfilled and alumina oxide filled 828DEA epoxy.

Table of Contents

List of Figures

List of Tables

1. Introduction

The adhesive properties and stiff, viscoelastic mechanical response of glassy thermosets distinguish them from other materials and make them versatile in many applications. Thermosets (e.g., epoxies) are often used in electronic packaging as encapsulants for structural integrity and high voltage isolation, adhesives for bonding piece-parts together, and underfills to attach surface mounted components to printed circuit boards. Figure 1 shows a schematic of an electronic package which makes use of epoxies as an overpot and adhesive underfill. Although stress relief coatings are typically elastomers, the composite printed circuit boards (PCB) also are usually made from filled thermosets stacked in layers.

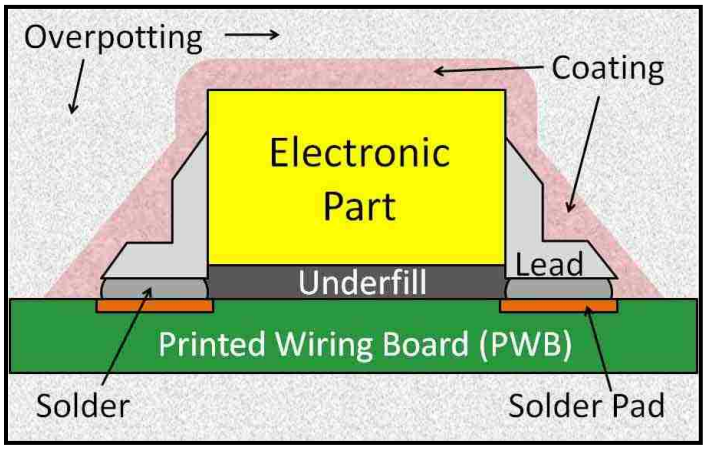

Figure 1 - Schematic of Electronic Packaging Materials

Surface mounted components that are soldered to PCBs often encounter thermal environments and dynamic loading conditions that may cause catastrophic failure of solder joints breaking electrical connections important to the function of the assembly. To remedy this problem, epoxies are often used as an underfill to create a strong bond between the surface mounted component and PCB providing stress relief to the solder

joint. Unfortunately, epoxies are complex materials that can exhibit highly nonlinear behavior when subjected to various thermal and mechanical environments. This makes it increasingly important for designers to be able to accurately predict how these materials will perform under the diverse service conditions encountered in a product life cycle. Accurate material models and knowledge of potential failure mechanisms are needed to predict design margins.

This thesis seeks to predict the adhesive strength of a bonded joint as part of a project investigating electronic packaging survivability. This will be done by correlating experimental failure data to computational stress-strain predictions using a well characterized nonlinear viscoelastic (NLVE) material model developed at Sandia National Laboratories. Computational tools will be used to evaluate a predictive failure metric for the epoxy to determine whether it can be applied to other applications undergoing various modes of loading.

2. Review of Related Literature

2.1. Potential energy clock model

A well characterized and extensively validated NLVE constitutive model known as the Potential Energy Clock (PEC) model has been developed at Sandia National Laboratories to predict the stress-strain response of polymers. The PEC model is derived using the Helmholtz free energy and incorporates a "material clock" through which potential energy accelerates polymer relaxations [1]. The PEC model was initially evaluated using experimental data from a wide array of tests. The experiments measured stress-strain response and change in material properties due to temperature over time for four different polymers. Predictive capabilities of the model showed near quantitative agreement for volume and enthalpy relaxation as well as accurate stress-strain behavior including yield [2]. The PEC model has since been used to accurately predict a wide range of responses including: temperature dependent yield under different modes of loading, change in apparent glass transition temperature with pressure, a smooth transition between the glassy and rubbery heat capacities and coefficients of thermal expansion, enthalpy relaxation, increase in the yield stress with time, tensile creep at different temperatures and cooling rates, and coupled effects such as extreme enthalpy relaxation after application of large stresses.

2.2. Simplified potential energy clock model

While the PEC model has shown great accuracy in its predictive capabilities, it is also complex and difficult to parameterize. The Simplified Potential Energy Clock model (SPEC) was created to reduce the complexity of the PEC model by eliminating less

important temperature-volume dependencies, decoupling the material clock and constitutive equation, and simplifying the strain measure used in its derivation [3]. Only the terms necessary for accurate predictions remain. These simplifications make the SPEC model more phenomenological than the PEC model and reduce the amount of experimental data needed to parameterize the constitutive equation. The resulting SPEC constitutive equation to calculate stresses in glassy thermosets is

$$\begin{aligned}\underline{\underline{\sigma}} = \frac{\rho}{\rho_{ref}}\left[K_d(T)\int_0^t ds\ f_v(t^*-s^*)\frac{dI_1}{ds} - L_d(T)\int_0^t ds\ f_v(t^*-s^*)\frac{dT}{ds}\right]\underline{\underline{I}} \\ + \frac{2\rho G_d(T)}{\rho_{ref}}\int_0^t ds\ f_s(t^*-s^*)\times\left[\underline{\underline{R}}(t)\cdot\underline{\underline{d}}_{dev}(s)\cdot\underline{\underline{R}}^{-1}(t)\right] \\ + \frac{\rho}{\rho_{ref}}\left[K_\infty(T)I_1 - L_\infty(T)\{T-T_{ref}\}\right]\underline{\underline{I}} + \frac{2\rho G_\infty(T)}{\rho_{ref}}\left[\underline{\underline{R}}\cdot\underline{\underline{\varepsilon}}_{dev}\cdot\underline{\underline{R}}^{-1}\right]\end{aligned} \quad (1)$$

where "material time" $t^*-s^* = \int_s^t \frac{dx}{a(x)}$, and the "shift factor" a is, $\log(a) = -\frac{C_1 N}{C_2 + N}$

where
$$\begin{aligned}N = &\left[\{T-T_{ref}\} - \int_0^t ds\ f_v(t^*-s^*)\frac{dT}{ds}\right] + C_3\left[I_1 - \int_0^t ds\ f_v(t^*-s^*)\frac{dI_1}{ds}\right] \\ &+ C_4\int_0^t\int_0^t dsdu\ f_{ss}(t^*-s^*, t^*-u^*)\,\underline{\underline{d}}_{dev}(s):\underline{\underline{d}}_{dev}(u)\end{aligned}$$
.

$\underline{\underline{\sigma}}$ is the Cauchy stress, $\underline{\underline{d}}_{dev}$ is the deviatoric unrotated rate of deformation tensor, $\underline{\underline{\varepsilon}}$ is its integral with first invariant, I_1, T is temperature, T_{ref} is the reference temperature where all coefficients and spectra are defined, ρ is density (ρ_{ref} is the density at the arbitrary, unstrained reference state), and $\underline{\underline{R}}$ is the rotational component of the deformation gradient. Although the formulation is rheologically simple, material time is used to alter relaxation rates based on the potential energy history. The required material properties include the decaying and equilibrium bulk and shear moduli (K_d, K_∞, G_d, G_∞), the

decaying and equilibrium products of bulk moduli and coefficients of thermal expansion ($L_d = K_d\alpha_d$, $L_\infty = K_\infty\alpha_\infty$), two relaxation spectra corresponding to the volumetric and shear terms (f_v, f_s), and two Williams-Landel-Ferry (WLF) coefficients (C_1, C_2). In all cases, the decaying terms are defined as the difference between the glassy and rubbery quantities. The volumetric and shear spectra, f_v and f_s, are defined by stretched exponential functions seen in Equation 2 and are then expanded as a Prony series in computational codes to simplify their integration (Equation 3). The constants τ and β are constants obtained from experimental data.

$$f_{v,s}(t) = e^{-(t/\tau)^{\beta}} \tag{2}$$

$$f_{v,s}(t) = \sum_k f_k e^{-t/\tau_k} \tag{3}$$

Two parameters, C_3 and C_4, describe (among other phenomena) the pressure dependence of the glass transition and the acceleration of relaxation rates under applied deformations that produces yield.

Evaluation of the SPEC model as well as its comparison to the PEC model is performed in [4]. Although greatly simplified, the SPEC model agrees well with the PEC model and shows accurate predictions across a wide range of tests similar to those originally predicted by the PEC model in [2].

2.3. Generic filled SPEC model

There are many types of epoxies that can be created from mixtures of different resins, hardeners, and fillers such as glass micro balloons (GMB) and aluminum oxide (AlO_x) particles. A designer would like to predict what material properties and filler volume

fractions would be ideal for a specific application. Moreover, sometimes property measurements are unavailable for an analysis. To assist in that goal, a generic SPEC model was created employing default properties that could be used when material properties for a thermoset are not known. Research at Sandia National Laboratories has shown that crosslinked epoxies have very similar properties when normalized about their respective glass transition temperature (T_g) [4]. This phenomena holds true even when the T_g of the epoxies differ by 150C from each other. Justified by these findings, the SPEC model was configured to default to a fixed set of properties taken from an unfilled Epon 828 epoxy resin and diethanolamine curative (828DEA). However, the user was required to define $T_{ref} = T_g + 10$ based on the value of T_g for the material.

To accomadate the effect of fillers, it was noted that experimental data in [4] determined that when the moduli of the filler are significantly greater than the moduli of the epoxy, the newly created composite properties, Ψ, could be approximated using a rule of mixtures seen in Equation 4.

$$\Psi = \Psi_e(1-\phi)^x \tag{4}$$

The subscript 'e' denotes epoxy properties, 'x' is an experimentally determined exponent, and ϕ is the filler volume fraction. Using this functional form derived from experimental observation, moduli and thermal expansion coefficients of a general filled epoxy can be defined by specifying the filler volume fraction of the material. The generic filled SPEC model predictions line up well with experimental data for typical unfilled and filled epoxy systems. The generic filled SPEC model gives an engineer the unique ability to

make reasonable performance predictions knowing only two properties of an epoxy, T_g and the amount of filler present in the mixture.

2.4. Failure predictions using the SPEC model

The SPEC model has been used to propose a failure metric for glassy themosets. Cohesive failure experiments were performed on notched 3-point bend, notched dog-bone, compression, and creep tests at various temperatures using 828DEA epoxy. The failure data from these tests was compared to FEA predictions using the SPEC model [5]. It was noted that any stress based metric would not predict failure in creep tests since stresses can be held constant and still cause failure due to relaxation of the epoxy over time. Alternatively, a strain based metric could apply to all tests including creep. It was hypothesized that maximum principal strain (EPSMAX) might work because it represents the largest strain state. Using FEA and the SPEC model, EPSMAX versus load was plotted for the element showing the largest value of EPSMAX near the time of failure seen in experiments. A significant increase in strain (yielding) was noticed when the macroscopic load in the analysis reached a critical value. This significant increase in strain is referred to as "runaway viscoelasticity" and it represents a rapid stress relaxation of the thermoset as monomer chains reorient themselves. The predicted load at the onset of runaway viscoelasticity compared reasonably to the experimental load at failure for all of the different tests performed. It was postulated that a value of EPSMAX near the onset of runaway viscoelasticity could be used to predict the initiation of cohesive failure for glassy thermosets. It was found that a EPSMAX value of roughly 40% captured cohesive failure predictions in problems with bounded strain gradients within reasonable engineering accuracy for all tests [5].

The SPEC model has also been previously used to determine if EPSMAX can be used as a failure criterion to predict the initiation of de-bonding in adhesive failure experiments. To initiate adhesive failure, a napkin ring test geometry was used for its unique ability to produce a nearly uniform stress state during shear loading. An example of a napkin ring test coupon can be seen in Figure 2.

Figure 2 - Napkin Ring Test Coupon

Other standardized test geometries such as lap shear or butt tension samples involve complicated stress distributions due to high strain gradients at the substrate-air-adhesive corner (i.e., at elastic singularities). The absence of such severe stress risers in napkin ring geometries make converged numerical solutions and accurate predictions in FEA more likely. Adhesive de-bonding of thermoset materials were examined in napkin ring tests (torsional ramp and creep at various temperatures) and correlated to SPEC model predictions in FEA [6]. It was found that an element at the de-bonding surface interface exhibited runaway viscoelasticity at the point of experimental failure. Napkin ring samples failed at different values of engineering strain depending on the type of test (torsional ramp or creep), but a predicted value of maximum principal strain (EPSMAX)

near the onset of runaway viscoelasticity was able to capture, within reasonable engineering accuracy, all napkin ring test data (25% strain [6]). This demonstrated that EPSMAX near the onset of runaway viscoelasticity was also capable of predicting adhesive failure of thermosets.

2.5. Previous electronics survivability investigations

Previous efforts have been made to develop a fundamental understanding of the behavior of electronic components and packaging systems exposed to thermal environments and dynamic loads. Mismatches in thermal strain among thermoset underfills and overpots, elastomeric stress relief coatings, and other types of materials in an electronic package produce stresses capable of failing the solder joint connecting a surface mounted component to a PCB. The underfill in particular is capable of producing stresses that cause thermal mechanical fatigue of the solder joint. The solder fatigue life due to the strains incurred from variations in an unfilled and filled (GMB, AlO_x) 828DEA epoxy underfill was investigated in [7] using the Solomon's Coffin Manson failure criteria. The unfilled SPEC and general filled SPEC models were used for the nonlinear viscoelastic stress-strain predictions of the underfill material. It was determined that an underfill could improve solder fatigue life based on the amount and type of filler added to the underfill. The predictive capabilities of the SPEC model make design for solder survivability possible.

While an underfill is capable of producing stresses that can fail a solder joint, it is acknowledged that an underfill may also be necessary for its survival. An underfill is the primary adhesive bond between a surface mounted component and PCB that provides stress relief to the solder joint during PCB deformation. For that reason, preliminary

investigations into underfill survivability have been performed at Sandia National Laboratories. Experiments using a small number of test coupons similar to test coupons used in the experimentation of this thesis were compared to FEA predictions using the SPEC model. It was determined that predictions were not sensitive on the macroscopic level (Load vs. Displacement), but local stress-strain predictions in the underfill were sensitive to mesh refinement and the geometry of the epoxy bond. The ability to predict underfill failure was not concluded. Additional experimental data and more accurate modeling of the test coupon was needed to assess a potential failure criteria. That is the goal of this thesis.

3. Experimentation

The following section will outline an experiment to simulate adhesive failure of a polymer underfill due to an applied mechanical load. Later, computational analyses will be carried out to simulate the experiments using the SPEC model. Comparison of the following experimental test to computational analyses will answer the question of whether maximum principal strain in analyses can be used to predict the initiation of adhesive failure of thermosets under combined modes of loading on a sample with complex geometrical features.

3.1. Test coupon preparation

Performing experiments on a realistic electronic package can complicate computational predictions due to the material interactions of many different parts in the assembly. For this reason, a mock electronic packaging test coupon was created to isolate the material response of an epoxy underfill. The coupon will simulate some of the geometrical features found in an electronic package assembly. Coupons are created by bonding a stainless steel plate to a stainless steel cylinder with an unfilled and 40vol% aluminum oxide (Almatis, Alumina A20 SG) filled 828DEA epoxy. Stainless steel is used for the bonded parts because it is significantly stiffer than 828DEA. This ensures that the NLVE response of the assembly during testing is due to the stress relaxation of the epoxy bond and not adjacent materials. The coupon can be seen in Figure 3.

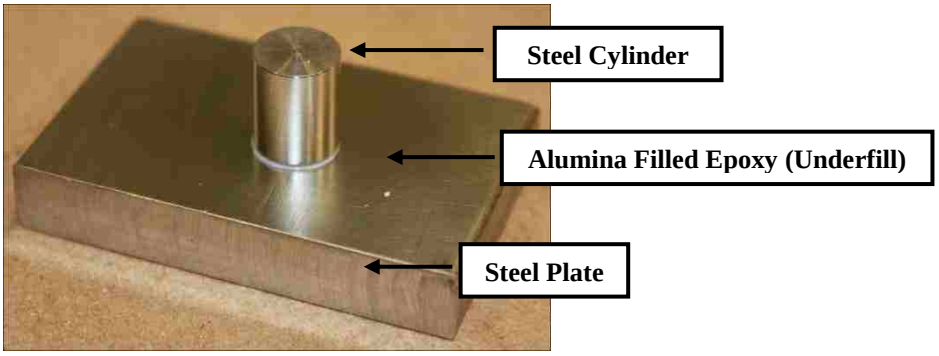

Figure 3 - Mock Electronic Package Test Coupon

To create test coupons, a fixture is set up that will hold coupon parts during assembly and restrain the coupons during cure of the epoxy bond. The coupon curing fixture can be seen in Figure 4. Previously cut cylinders (D = 0.375", H = 0.5") and plates (2”x1.25”x0.3125”) are cleaned with isopropyl alcohol to remove debris that can contaminate adhesion of the epoxy bond. The plates are attached to the lower half of the fixture with tape while the cylinders are held in the upper half of the fixture with hand tightened screws (Figure 5).

828DEA epoxy is created from a mixture of diglycidyl ether of bisphenol A (Epon 828, DGEBA) cured with diethanolamine (DEA, Fisher Scientific) at a ratio of 100-to-12 parts-by-weight. Epon 828 is the monomer filled resin and DEA is the hardener that initiates crosslinking when mixed. The two parts are mixed at an elevated temperature of 71C to speed the crosslinking reaction of the epoxy. The mixture is then degassed in a heated vacuum chamber at 71C until there are no more bubbles evacuating from the mixture. When creating alumina filled epoxy (AlO_x) bonded coupons, alumina particles are thoroughly mixed into the Epon 828 and DEA mixture at an elevated temperature of 71C as well. However, the AlO_x mixture is not degassed because the mixture is too viscous to release any air bubbles. The unfilled or alumina filled 828DEA epoxy mixture

is then poured into a syringe and applied to the cylinders fixed in the upper half of the fixture. The upper half of the fixture with cylinders, is lowered onto the plates attached to the lower half of the fixture (Figure 6). Thickness of the underfill is determined by spacers placed between the upper and lower halves of the fixture. For this experiment, spacers 0.01" thick were placed between the two halves of the fixture to simulate a thin bond line typically used when bonding an electronic part to a PCB in a real electronic package assembly. The whole fixture and samples are placed in an oven at 71C for 26hrs (1hr for heat up, 24hr cure, 1hr cool down) for polymerization of the epoxy to occur. Samples were then taken out of the oven for testing.

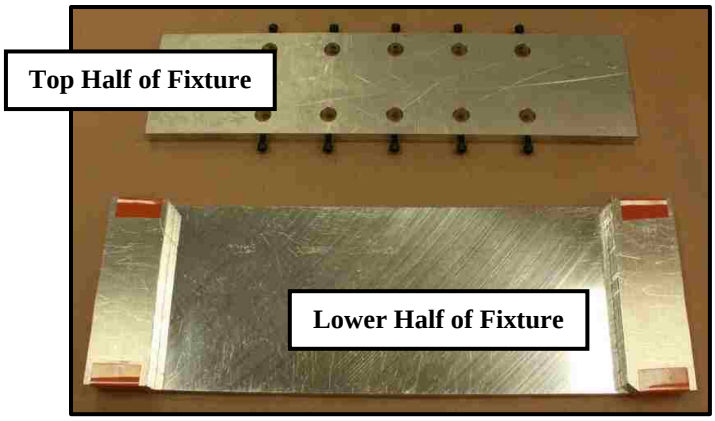

Figure 4 - Coupon Curing Fixture

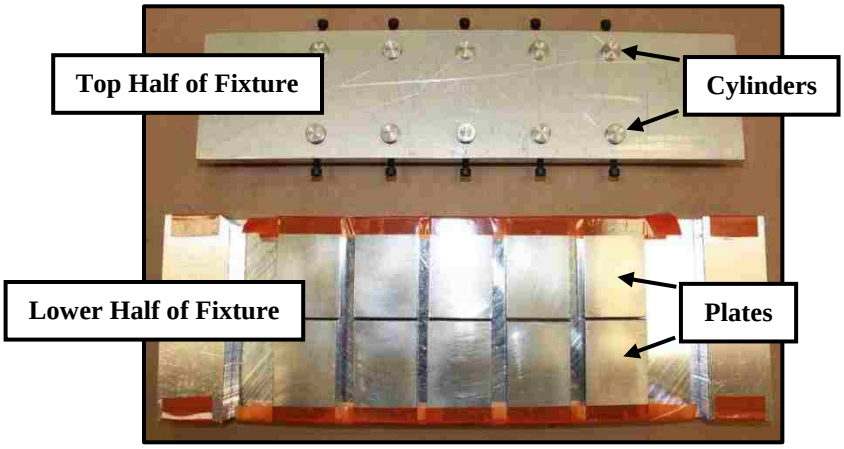

Figure 5 - Coupon Curing Fixture w/ Cylinders and Plates

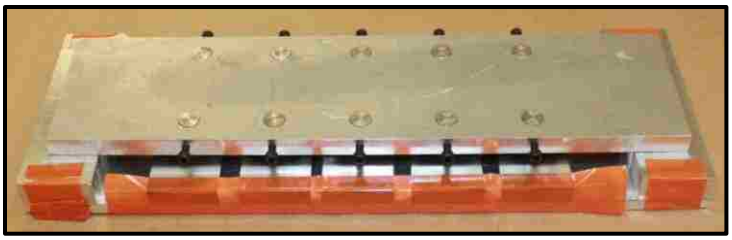

Figure 6 - Mated Fixture Halves

3.2. Cylinder push-off test

Testing each coupon was performed by moving a steel pusher attached to an Instron 5882 screw drive test frame downward at a rate of 0.01"/min into the cylinder until failure of the epoxy bond (Figure 7). A ±50kN load cell was used for obtaining reaction force data. Samples were held down with clamps during loading (Figure 8). Unfilled and 40vol% AlO_x epoxy bonded coupons were tested at five different pusher heights (H = 0.025", 0.105", 0.180", 0.260", and 0.374") to vary between a shear and tensile/bending mode of loading. All tests were performed at room temperature (≈22C). An average of 23 samples were tested for unfilled and 40vol% AlO_x epoxy at each pusher height. Load at failure, location of failure initiation, and bond thickness of each sample was recorded.

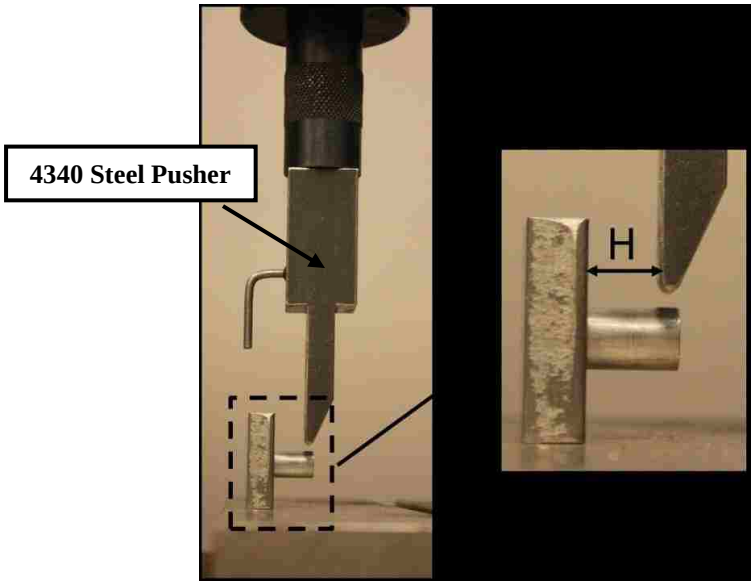

Figure 7 - Experiment Instron Setup and Pusher Height "H"

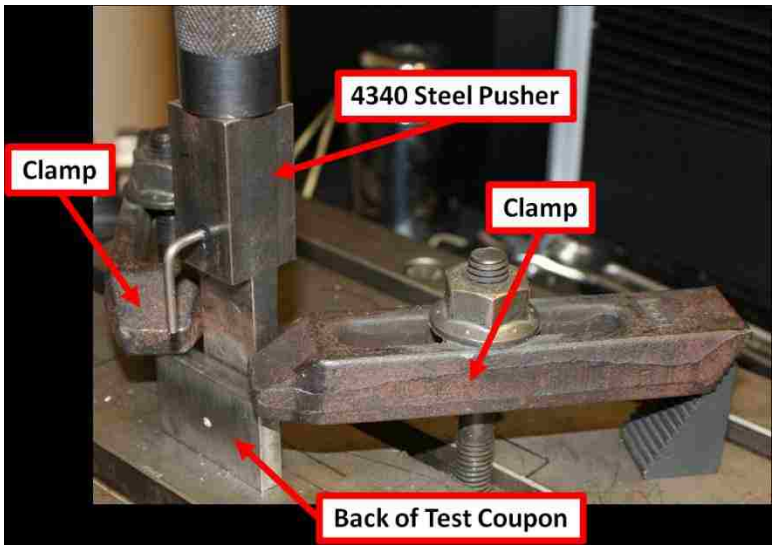

Figure 8 - Coupon Clamped on Instron

3.2.1. Reusing cylinders and plates

The experiments performed on the coupons did not appear to affect the surface finish of the adhered surfaces on the cylinder or plate. Therefore, to save on material the cylinder and plate were reused for additional tests. The cylinders and plates are soaked in N-Methylpyrrolidinone (NMP) which causes any remaining epoxy to swell and soften which releases the epoxy from a bonded surface. After the epoxy has released, the cylinders and plates are bathed in isopropyl alcohol to remove the NMP. The plates and cylinders were then scrubbed with an abrasive Brillo pad to remove any remnant epoxy particulates. To finish, the cylinders and plates are soaked in isopropyl alcohol and wiped clean. The cleaning process did not appear to affect the surface conditions of the steel components. The cylinders and plates were then ready for reuse.

3.3. Cylinder push-off test results

All tested coupons showed evidence of the epoxy de-bonding from the cylinder interface directly beneath the contact region of the pusher. Coupon failure can be seen in Figure 9

through Figure 13. The pusher moved in the same direction on each sample indicated by an arrow drawn in some of the figures. The positions of the cylinders in each figure do not necessarily match the position of the plate. The cylinders are shown so that the location of the epoxy absent from the plate can be visualized. Upon failure, any epoxy not on the plate was on the cylinder. Failure initiation in all coupons appeared to be adhesive and in many cases would de-bond along the interface of failure. However, in some cases failure of the epoxy bond would result in a crack that propagated through the bulk of the epoxy material from the cylinder interface to the plate interface. An example of this can be seen in Figure 14 where failure initiates and propagates adhesively along the cylinder interface, cracks cohesively through the epoxy, and then continues its adhesive failure along the plate interface. Although failure may appear to be cohesive it can still be said that the epoxy bond failure is adhesive because failure initiates and initially propagates along an interface. Crack propagation after failure initiation can be wildly unpredictable and should not detract from an otherwise adhesive failure initiation mechanism.

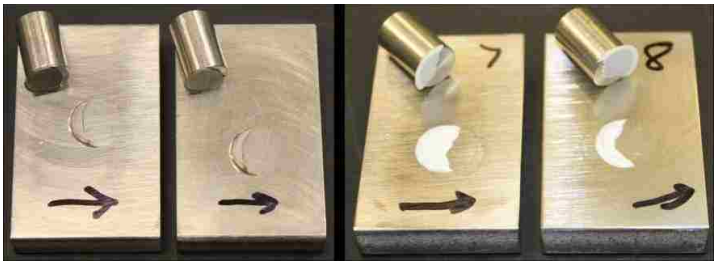

Figure 9 - Failure at H = 0.025" (unfilled at left, 40vol% alumina filled at right)

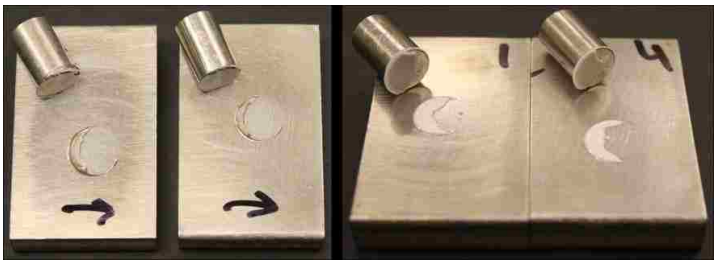

Figure 10 - Failure at H = 0.105" (unfilled at left, 40vol% alumina at right)

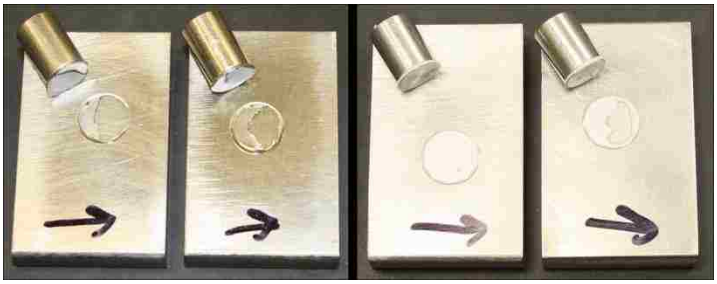

Figure 11 - Failure at H = 0.180" (unfilled at left, 40vol% alumina at right)

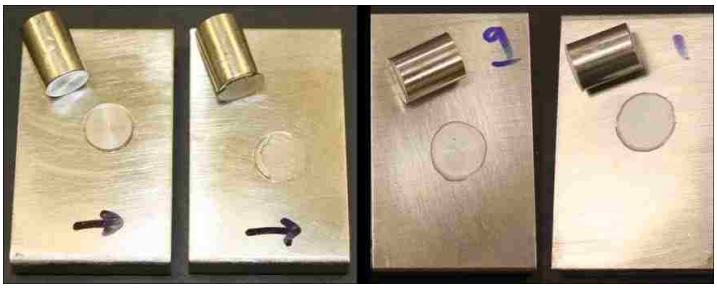

Figure 12 - Failure at H = 0.260" (unfilled at left, 40vol% alumina at right)

Figure 13 - Failure at H = 0.374" (unfilled at left, 40vol% alumina filled at right)

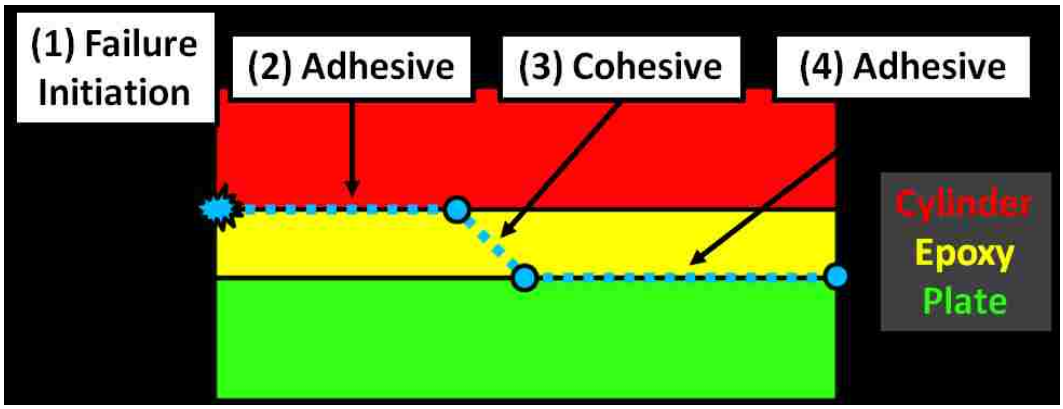

Figure 14 – Experiment Failure Initiation Example

The average load at failure and error bars representing standard deviation at each pusher height is displayed in Figure 15. A table of the experimental data from Figure 15 can be seen in Table 1. The trend in the data shows that the average load at failure decreases with an increasing pusher height. Alumina filled epoxy typically failed at a higher load than their unfilled counterpart at each pusher height. However, load at failure of alumina filled samples were similar to unfilled samples within one standard deviation which does not suggest a large bonding strength increase from adding hard filler.

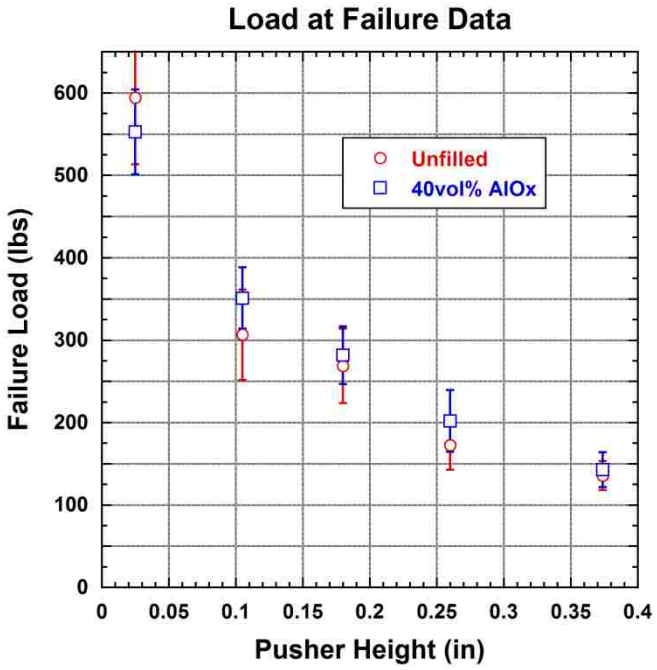

Figure 15 - Load at failure for each pusher height

Table 1 - Experimental Data for Push Off Test

Pusher Height (in)	Unfilled 828DEA		40vol% AlO_x 828DEA	
	Avg. Failure Load (lbs)	Std. Dev. (lbs)	Avg. Failure Load (lbs)	Std. Dev. (lbs)
0.025	594.10	80.51	550.86	51.49
0.105	306.31	54.75	350.28	37.42
0.180	268.40	45.15	281.58	34.98
0.260	172.53	29.86	202.00	37.47
0.374	132.51	17.74	156.25	25.97

The standard deviation at each pusher height can be almost 20% from the average failure load. Inconsistencies in the data are most likely due to small geometrical variations of the epoxy bond in each sample as well as the surface condition of the cylinder bonded to the plate. The variation in bond thickness of each coupon was one variable that was difficult to accurately maintain. Although a 0.010" spacer was placed between the two halves of

the coupon curing fixture, the average bond thickness was 0.013"±0.002". Data seen in the appendices of this thesis show that small variation in thickness were not producing obvious trends in the failure loads for each pusher height. At any given pusher height, it could be seen that 0.010” and 0.015" thick epoxy bonds had similar average failure loads and similar standard deviations from that average. For this reason, small variations in bond thickness were considered to be negligible in its contribution to the spread in experimental data. However, all of the coupons showed varying amounts of epoxy wetting up the side of the cylinder along with varying epoxy area coverage on the plate. Ideally the contact area of the epoxy bond is the same on both the cylinder and plate, but variable wetting on both surfaces is inevitable.

A cross section view of the sample seen in Figure 16 shows a close-up view of a coupon at the edge of the cylinder and epoxy bond line. The cross section shows wetting of the epoxy on the side of the cylinder and larger contact area on the plate than cylinder surface. The cross section also shows a chamfer on the cylinder which is a result of de-burring the cylinders by hand. Because all the cylinders were de-burred by hand, it is possible that the chamfer on each cylinder is slightly different which could be an additional source of experimental error. Sensitivity analyses were performed to examine data variability due to the variability of epoxy wetting as well as differences in cylinder geometry.

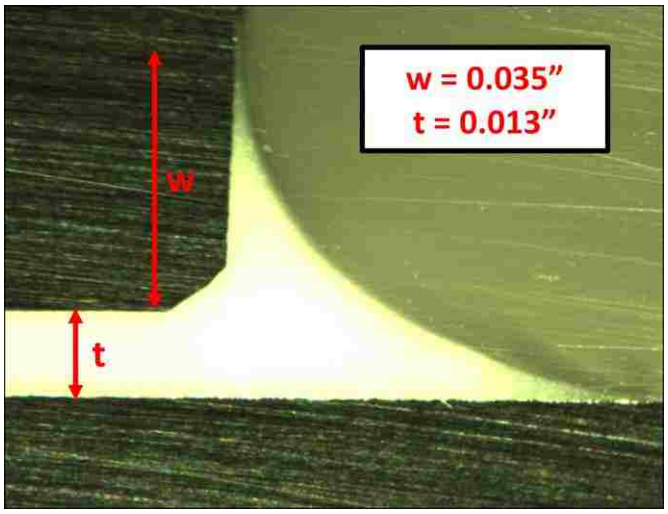

Figure 16 – 7.5x Zoom Cross Section of Coupon w/ Chamfer (0.013” thick bond, 0.035” wetting on cylinder wall)

3.3.1. Cylinder Geometry Sensitivity Test and Results

The surface conditions and variable chamfer of the cylinders were also investigated. The cylinders used in all samples were cut from stainless steel dowels on a lathe and lightly de-burred by hand with a file. Although the surfaces of the cylinders felt smooth they had a noticeable rough, machined appearance. As machine polished with rounded edge cylinders became available, a batch of samples was created and tested to compare against the samples with rough cut cylinders. A cross section of a machine polished and rounded edge cylinder coupon can be seen in Figure 17. The polished cylinders were then sandblasted (60 Grit Garnet) and tested to determine if a deliberately roughened surface could affect load at failure. A final batch of samples performed on machine polished with rounded edge cylinders were purposely left oily after machining to examine how surface contaminants may affect epoxy bonding strength. This comparison, seen in Figure 18, was performed with 40vol% AlO_x epoxy bond coupons at a pusher height of 0.025".

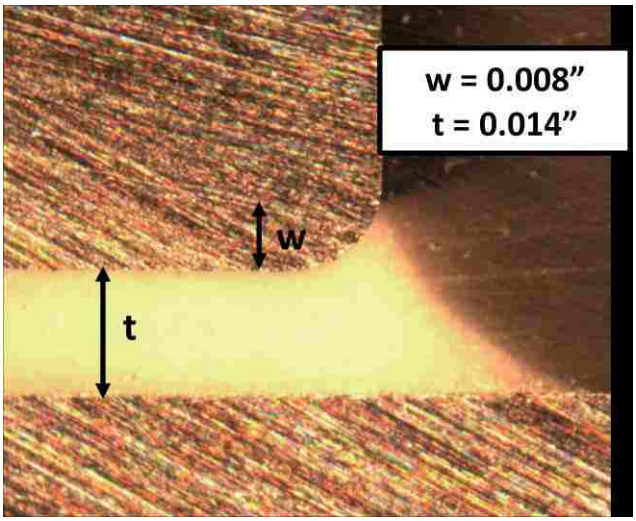

Figure 17 – 7.5x Zoom Cross Section of Coupon w/ Round (0.014” thick bond, 0.008” wetting on cylinder wall)

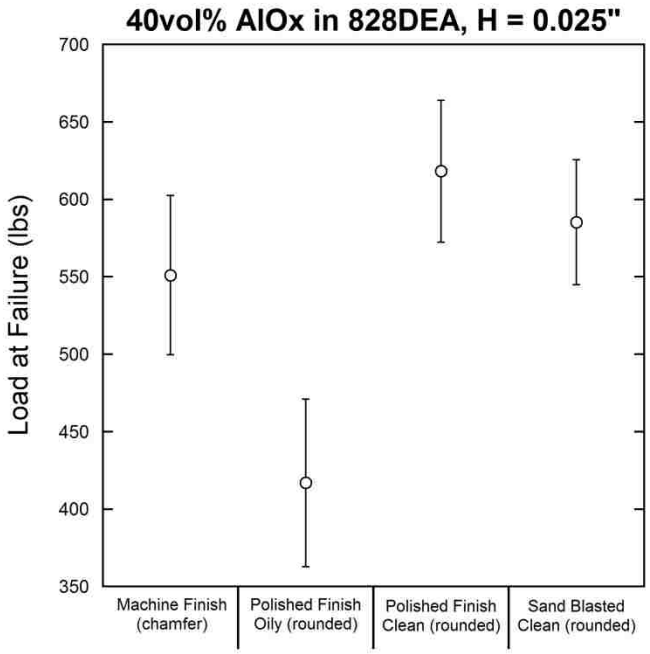

Figure 18 - Cylinder Surface Condition Comparison (40vol% AlO_x at H = 0.025")

Data from this comparison shows similar load at failure between the rough machined finish, clean machine polished, and sand blasted surface cylinder samples. However, the oily surface cylinder samples showed a large deviation from the other types of surface effects examined. The data shows that the load at failure is not so much affected by the

roughness or chamfer/rounded shape of the cylinder, but can be severely affected by contaminants on the cylinder surface.

3.3.2. Epoxy Wetting Sensitivity Test and Results

After examining the cross sections in Figure 16 and Figure 17, it was noticed that the amount of wetting can vary significantly between coupons. To examine the sensitivity of load at failure due to differences in epoxy wetting, samples were created that are purposely "messy" with a larger than normal wetting on the cylinder wall. The messy samples provide an extreme case of cylinder wetting and spread of the epoxy on the plate surface. Wetting is measured from the bottom of the cylinder to the highest visible point of the wetting on the cylinder wall. Measurements of the wetting of epoxy up the side of the cylinder showed a 0.022”±0.004” wetting for “normal” samples and 0.050”±0.006” wetting for “messy” samples The comparison between “normal” samples and purposefully "messy" samples were performed at a pusher height of 0.374". Data from this comparison are seen in Figure 19. Data shows that the difference between the average load at failure for normal and messy samples can differ by almost 25%.

It is also interesting to see that the standard deviation in failure loads is smaller for the messy samples than the normal samples. This could be from some critical value of wetting being reached in the messy samples resulting in more consistent data. Even though a large amount of epoxy was applied to the messy samples there was only so much epoxy the cylinder could be immersed in before excess epoxy flowed away from the cylinder and across the plate. In that sense, there is a limit to the amount of wetting that can occur on the messy samples. Messy samples were an extreme case of wetting that the normal samples never reached, but the comparison clearly illustrates how

experimental error can be caused by variable epoxy wetting on the cylinder and larger epoxy area coverage on the plate.

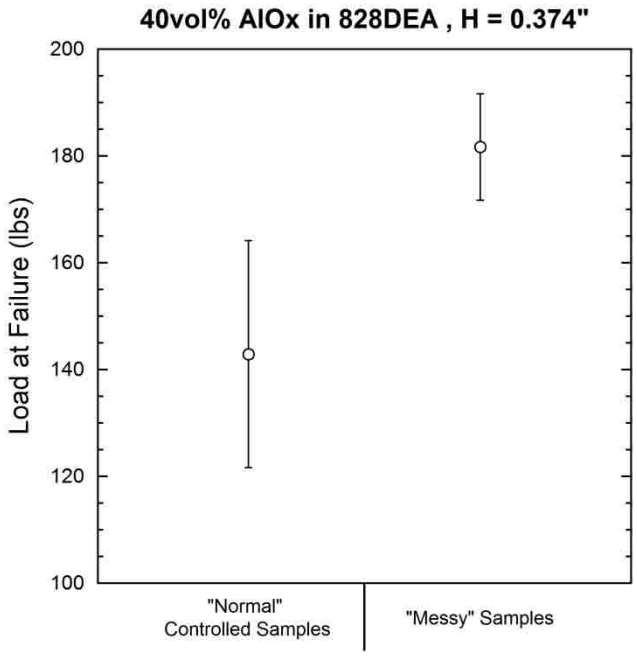

Figure 19 - Normal vs. Messy Created Samples, 40vol% AlO_x at H = 0.374"

3.4. Experimental Discussion

The cylinder push off test performed has a unique geometrical similarity to actual applications while providing adhesive failure data under mixed loading conditions. Adhesive failure of the epoxy bond is sensitive to many things including added fillers, epoxy bond geometry, and surface conditions of the bonded substrates. Epoxy bond geometry (thickness, wetting) varies among all coupons and is a source of experimental error. However, creating coupons with similar epoxy bond geometry is less important than the cleanliness of bonded surfaces when gathering experimental data. There are many possible sources of experimental error, but the observable trend in pusher height failure data speaks to a certain degree of coupon manufacturing consistency. Sensitivity tests have shown that geometrical variability may contribute a small amount of error on a

macroscopic level, but FEA will determine their importance on the localized level and if more consistent coupon geometries are necessary for accurate FEA predictions.

4. Finite Element Analysis (FEA) of Coupon

The following section outlines how the FEA model is created, the constitutive models used for each material, and the boundary conditions implemented to simulate the previously performed experiment.

4.1. FEA Software Package

Computational analysis of the mock assembly coupon was performed using a Sandia National Laboratories developed finite element software package, Sierra Adagio. Adagio is an implicit finite element package used for the analysis of solids and structures [8]. Adagio employs a multi-level iterative solver to solve problems with large deformations, nonlinear material behavior, and contact. Eight node hexahedral elements are used where nodal deformations are solved numerically using a one point gauss quadrature rule of integration. Each element has one integration point located at its centroid which makes stress or strain constant across the element. This makes mesh refinement around areas of interest important, but also allows for extraction of stress-strain predictions at precise locations.

4.2. FEA Model Creation

CUBIT is a full-featured software toolkit for robust generation of two- and three-dimensional finite element meshes and geometry preparation. CUBIT is used to create the computational model of the experimental setup and apply a finite element mesh to all geometries. The full model of the experimental setup can be seen in Figure 20. To reduce computational time in Adagio, the number of elements in the model will be reduced by using a half symmetry model seen in Figure 21.

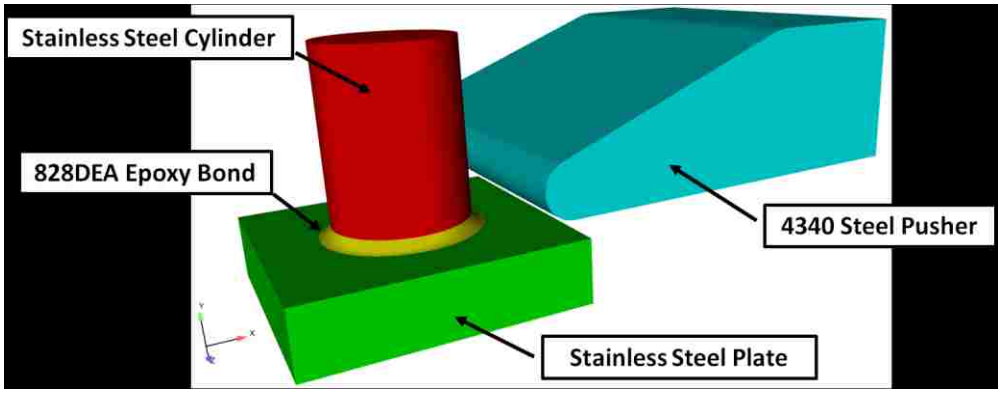

Figure 20 - Full Model of Coupon

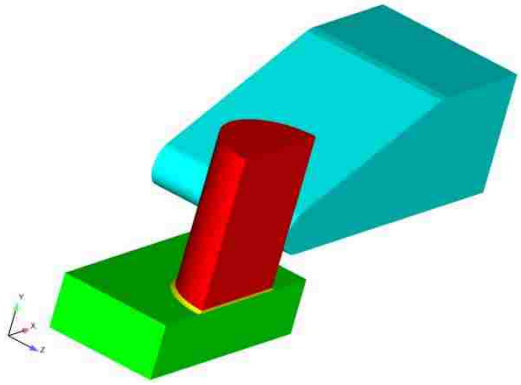

Figure 21 - Half Symmetry Model Coupon

4.3. Material Constitutive Models

4.3.1. Thermo elastic-plastic power law hardening constitutive model

Elastic and post yield response of the pusher, cylinder, and plate will be predicted using a thermo elastic-plastic power law hardening constitutive model. The post yield stress, $\overline{\sigma}$, is calculated by Equation 5 and has been implemented in Adagio as described in reference [9]. For all analyses, Lüders strain, ε^L, is set to zero and is neglected. Equivalent plastic strain, ε^p, is a function of the current strain of an element and is greater than zero after yield of the metal. Although each material property can be a function of temperature, the experiments were conducted at room temperature (22C) and

therefore remain constant with respect to room temperature. The stainless steel material properties used for the cylinder and plate are listed in Table 2. The 4340 steel material properties used for the pusher are listed in Table 3. It should be noted that the properties listed for the metals did not come from experimental testing. The metal properties were taken from a material data base and were assumed to match closely with the actual properties of the materials. The assumed properties are reasonable approximations for modeling purposes.

$$\overline{\sigma} = \sigma_{ys} + A\langle \varepsilon^p - \varepsilon^L \rangle^n \tag{5}$$

Table 2 - Material Properties of Stainless Steel (at 22C)

Youngs Modulus	E	194.392 GPa
Poissons Ratio	ν	0.264
Initial Yield Stress	σ_{ys}	205.929 MPa
Hardening Constant	A	864.644 MPa
Hardening Exponent	n	0.53574

Table 3 - Material Properties of 4340 Steel (at 22C)

Youngs Modulus	E	194.501 GPa
Poissons Ratio	ν	0.264
Initial Yield Stress	σ_{ys}	470.214 MPa
Hardening Constant	A	864.644 MPa
Hardening Exponent	n	0.53574

4.3.2. Simplified potential energy clock constitutive model

Nonlinear viscoelastic (NLVE) response of unfilled and alumina filled 828DEA epoxy will be predicted using the Simplified Potential Energy Clock model. The SPEC constitutive equation that calculates stresses in glassy polymers has been outlined in the

literature review section (Equation 1). The experimentally obtained material properties necessary for SPEC model implementation can be seen in Table 4. The reference density, ρ_{ref}, is the only property in the Table 4 that does not use a hard filler exponent, 'x'. The reference density for the 40vol% AlOx 828DEA is 2306 kg/m^3. Values of the constants necessary for the material clock can be seen in Table 5.

Table 4 - Material Properties for 828DEA

Variable	Unfilled Value	Hard filler exponent, x
ρ_{ref}	1176 kg/m^3	---
T_{ref}	75^{o}C	0
K_∞ at T_{ref}	3.2 GPa	-1
dK_∞/dT	-12 MPa/^{o}C	-1
linear α_∞ at T_{ref}	600 ppm/^{o}C	1.3
$d\alpha_\infty/dT$	0.4 ppm/^{o}C^2	1.3
G_∞ at T_{ref}	4.5 MPa	-2.5
dG_∞/dT	0 MPa/^{o}C	-2.5
K_g at T_{ref}	4.9 GPa	-1
dK_g/dT	-12 MPa/^{o}C	-1
linear α_g at T_{ref}	170 ppm/^{o}C	1.3
$d\alpha_g/dT$	0.2 ppm/^{o}C^2	1.3
G_g at T_{ref}	0.75 GPa	-2.5
dG_g/dT	-4.2 MPa/^{o}C	-2.5
τ_s	0.12 sec^{-1}	0
β_s	0.22	0
τ_v	6 sec^{-1}	0

Table 5 - SPEC material clock constants for 828DEA

Variable	Unfilled Value	Hard filler exponent, x
C_1	16.5	0
C_2	54.5^{o}C	0
C_3	1000^{o}C	0
C_4	8,000^{o}C	-3.75

4.4. FEA Boundary Conditions

Analysis will model the boundary conditions (BC) of the experiments as closely as possible including cool down of the coupons after cure, coupon restraint during testing, and displacement controlled loading of the pusher. Fixed displacement BCs will be applied normal to the face of the entire model in the xy-plane which will enforce symmetry conditions during the entire analysis (Figure 22). Analyses begin with cool down from cure temperature of the epoxy (71C) to room temperature (22C). Each material is allowed to contract with respect to their coefficient of thermal expansion during cool down. After cool down fixed displacement BCs will be activated on the two faces of the plate in the yz-plane which will prevent displacement of the coupon in the same manner that the clamps hold the coupon from moving in the experiments (Figure 23). Finally, a velocity is applied to the back of the pusher, moving it in the negative x-direction, at a rate of 0.01"/min which corresponds to the velocity of the pusher in the experiment. Contact BCs between the pusher and cylinder are active during this time. The pusher velocity continues until the predicted reaction force exceeds the load seen in the experiments.

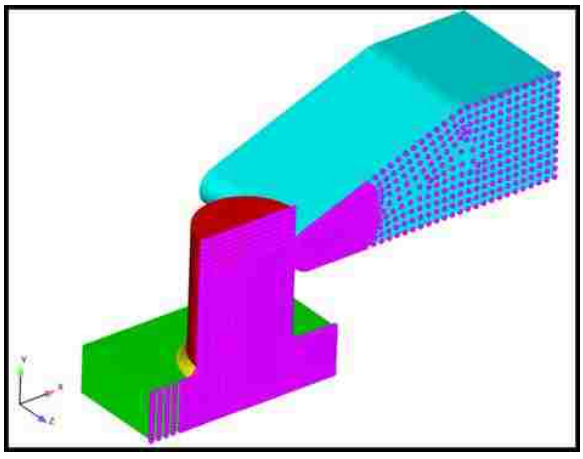

Figure 22 - Symmetry BC (purple spheres on nodes)

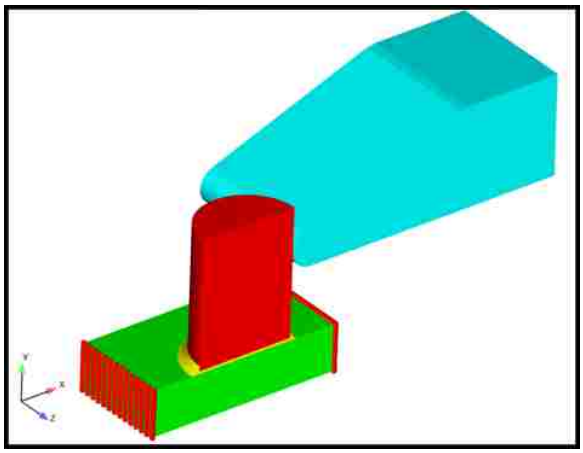

Figure 23 - Plate BC (red spheres on nodes)

4.5. FEA Simplifications

Certain aspects of the sample processing will be ignored in the analyses. The epoxy is a fluid until the hardener and resin have cured. Therefore, analyses will ignore the initial heat up of the sample. Cure stresses are not incorporated in the SPEC model and will not be a part of the analyses. However, residual thermal stresses due to CTE mismatch of the materials after cool down will be included in the analyses. All metals are assumed to be free of surface flaws and other inclusions. The 828DEA epoxy bond is assumed to be free of voids and homogenous when mixed with alumina hard filler. Analyses are assumed to be quasi-static due to the relatively slow change in temperature during processing and slow rate of displacement during testing. Therefore, small inertial effects are ignored. Friction forces due to the contact between the pusher and cylinder are neglected in computational calculations.

5. Determining an appropriate FEA model geometry

Wetting of the epoxy on the steel cylinder and epoxy wetting across the plate is difficult to control. However, it may not be necessary to model certain aspects of the epoxy bond geometry to accurately capture EPSMAX failure predictions. For this reason, idealized and realistic geometry models are investigated to assess the amount of detail that is necessary for converged stress-strain predictions. Mesh refinement studies for a 0.010" thick unfilled 828DEA epoxy bond at a pusher height of 0.260" was performed to determine spatial convergence for idealized and realistic geometry models. An attempt was made to be consistent when reducing the mesh size so as to make the elements in each refinement approximately half the size of the previous refinement. However, this was not always possible due to increasing geometrical complexity and the paving method used for meshing each model. The size of the elements in each refinement with respect to the initial mesh size is described for each geometry and should still allude to the likelihood of spatial convergence or lack thereof.

Data for unfilled 828DEA at H = 0.260" suggests that we are interested in predictions that correspond to a load of 172.53 lbs. Failure initiation is determined by an element in the epoxy bond displaying the largest EPSMAX at a predicted load corresponding to the experimental failure load. The location of predicted failure initiation at H = 0.260" for all idealized and realistic epoxy bond geometries can be seen in Figure 24. Convergence on a EPSMAX vs. Load plot and maximum principal stress (SMAX) vs ESPMAX plot will be investigated at an element corresponding to failure. SMAX and EPSMAX were chosen instead of other stress or strain metrics because they represent the largest stress or strain state at failure initiation. Moreover, previous adhesive and cohesive failure

research plotted SMAX vs. EPSMAX to determine yield or bending of the stress-strain curve which is indicative of runaway viscoelasticity. Plots of EPSMAX vs. Load were also used as a method of determining runaway viscoelasticity where strain would increase rapidly at some critical value of load. Convergence on these two plots will determine the ability to pick an accurate value of EPSMAX corresponding to an experimental failure load and if the load at which runaway viscoelasticity occurs is affected by mesh refinement.

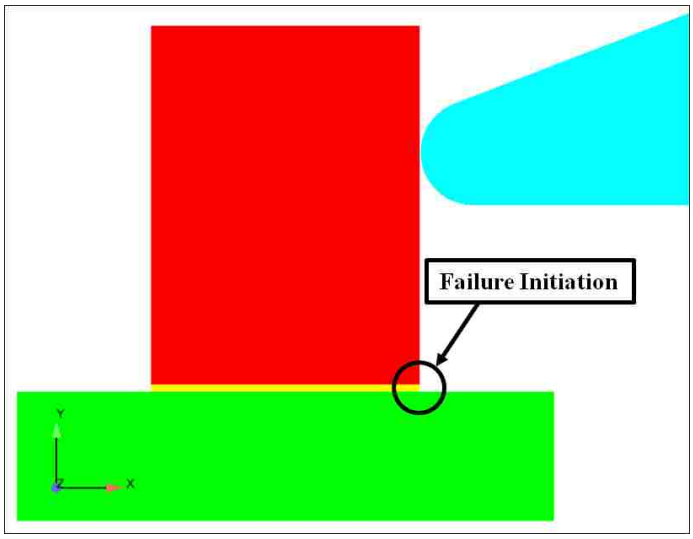

Figure 24 - Failure Initiation Location for Idealized and Realistic Geometries (H = 0.260")

5.1. Idealized epoxy bond geometry

Idealized fillet geometries are investigated because an engineer may choose to ignore geometrical complexities to save time during CAD design and simplify mesh refinement. The effect of neglecting cylinder and epoxy wetting geometrical features are investigated for a square, undercut, and overflow fillet epoxy bond seen in Figure 25. Note that Figure 25 and all subsequent mesh refinements of those geometries are a blow up of the failure

initiation site seen in Figure 24. All idealized cases assume that the cylinder has a square, sharp corner at the bond interface with no wetting on the cylinder.

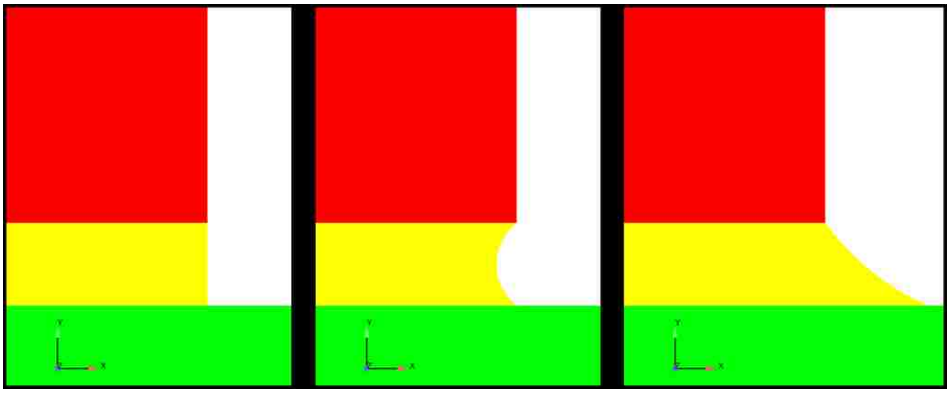

Figure 25 - Idealized Model Geometries (square, undercut, and overflow fillet)

5.1.1. Square fillet

The square fillet idealizes a case in which there is no wetting on the cylinder or plate. A fixed mesh resolution for the square fillet geometry was first used for preliminary analyses to determine model simplifications that can be made to reduce computational time of the simulations. The bond line mesh resolution for the following model simplification analyses can be seen in Figure 26.

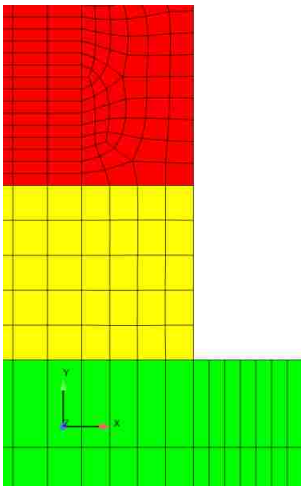

Figure 26 - Mesh Resolution for Model Simplification Analyses

A symmetry plane was originally proposed to reduce the number of elements, but if the cylinder is not bonded in the center of the plate or the pusher is not lined up perfectly with the cylinder in the experiments then the setup is not symmetrical. A model with the cylinder in the middle of the plate and pusher centered on the cylinder (Figure 27) is compared to a model with the cylinder offset on the plate and a pusher that is not centered on cylinder (Figure 28). This comparison will determine if the stress-strain predictions are sensitive to cylinder location on the plate and pusher location on the cylinder.

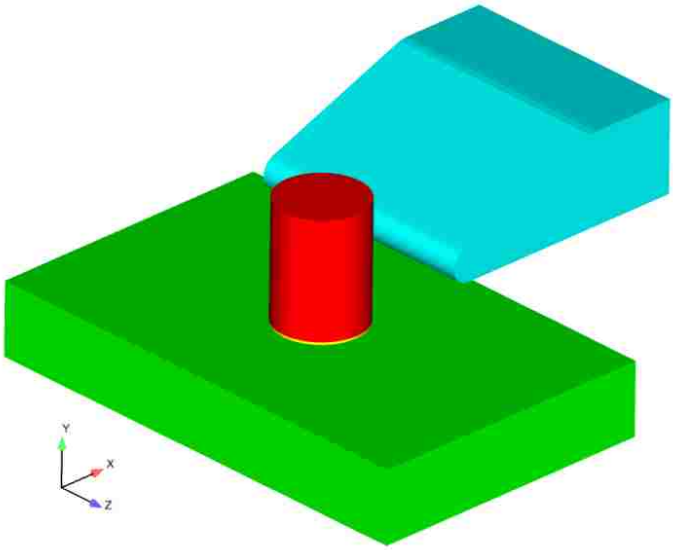

Figure 27 - Full Size Plate Model

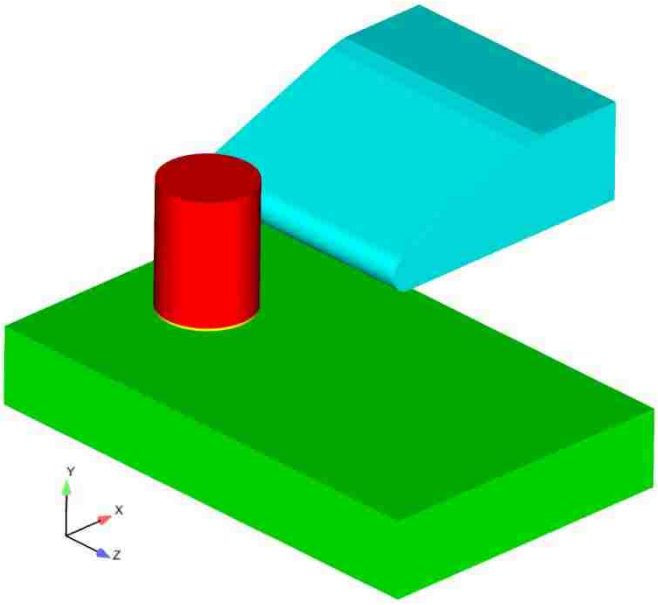

Figure 28 - Full Size Plate Model w/ Offset Cylinder and Pusher

An element in the epoxy bond displaying the largest EPSMAX at the time corresponding to experimental failure occurred in the same element in both models. Plots of EPSMAX vs. Load and SMAX vs. EPSMAX for that element can be seen in Figure 29 and Figure 30. Each plot shows that the predictions for the element of interest are identical. This affirms that the location of the cylinder on the plate and location of the pusher on the cylinder do not affect the solution. This also lends some validation to the fact that slight offsets in experiment test coupons will not affect the failure load either. All analyses will incorporate a half model with symmetry plane to reduce the number of elements in the model.

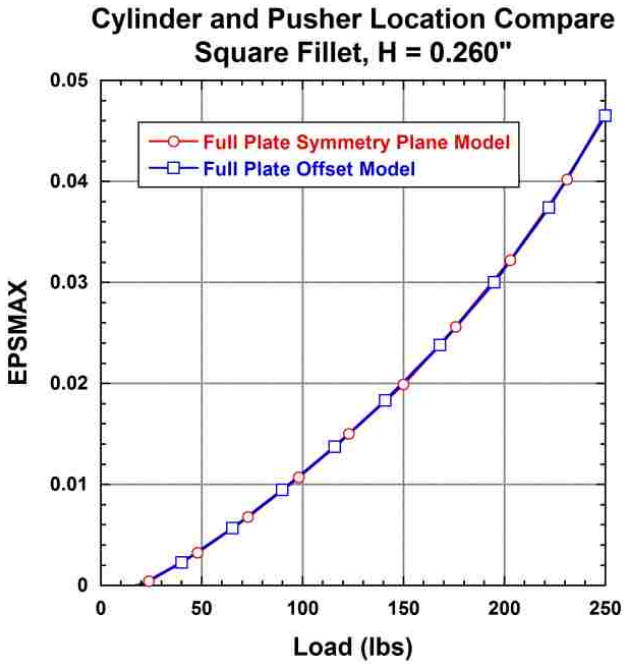

Figure 29 - Cylinder and Pusher Location Compare (EPSMAX vs. Load)

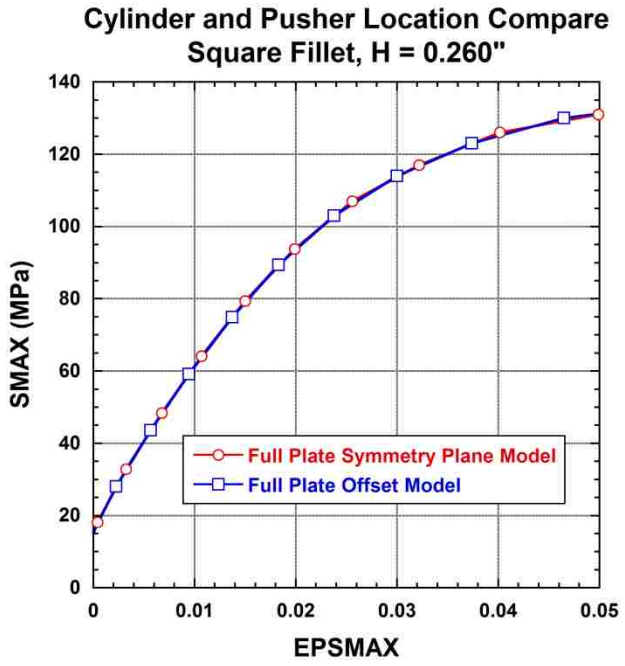

Figure 30 - Cylinder and Pusher Location Compare (SMAX vs. EPSMAX)

Although the number of elements is reduced by using a half model with symmetry plane, there are still many elements required to mesh the actual plate. To reduce the number of elements in the model further a smaller plate will be used in the model with the

assumption that the stress-strain response of the underfill is independent from the plate at some critical size of the plate. A comparison was performed between a model with the actual plate geometry (Figure 27) and a model with a smaller size plate geometry (Figure 31). The smaller plate geometry cuts all three dimensions (thickness, height, and width) in half.

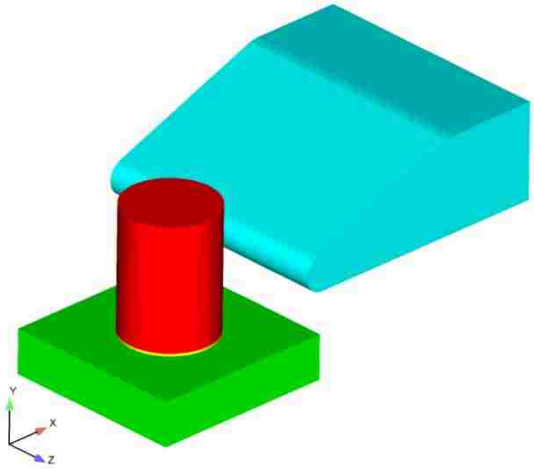

Figure 31 - Small Size Plate Model

An element in the epoxy bond displaying the largest EPSMAX at the time corresponding to experimental failure occurred in the same element in both models. Plots of EPSMAX vs. Load and SMAX vs EPSMAX for that element can be seen in Figure 32 and Figure 33. There is less than a 3% difference between the two model predictions of EPSMAX when the predicted load corresponds to experimental failure (172.52 lbs). The stress-strain curves are almost identical. All epoxy bond geometry models, including the square fillet case, will incorporate the smaller size plate to reduce the number of elements in the model.

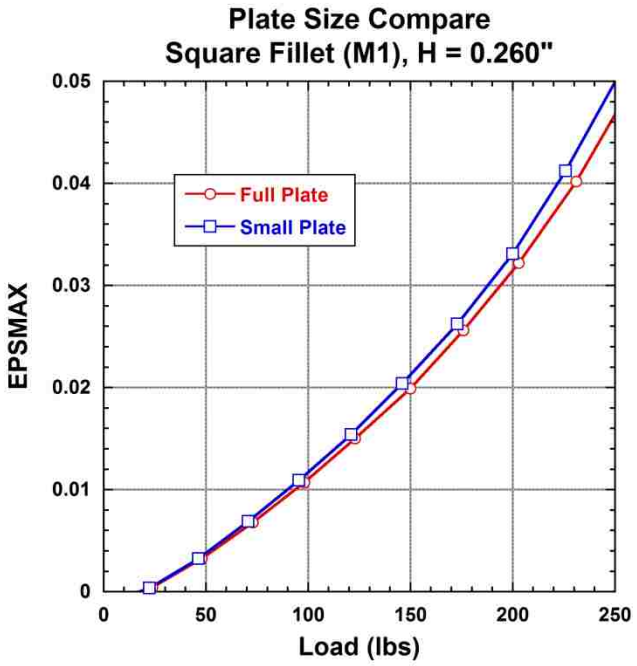

Figure 32 - Plate Size Comparison (EPSMAX vs Load)

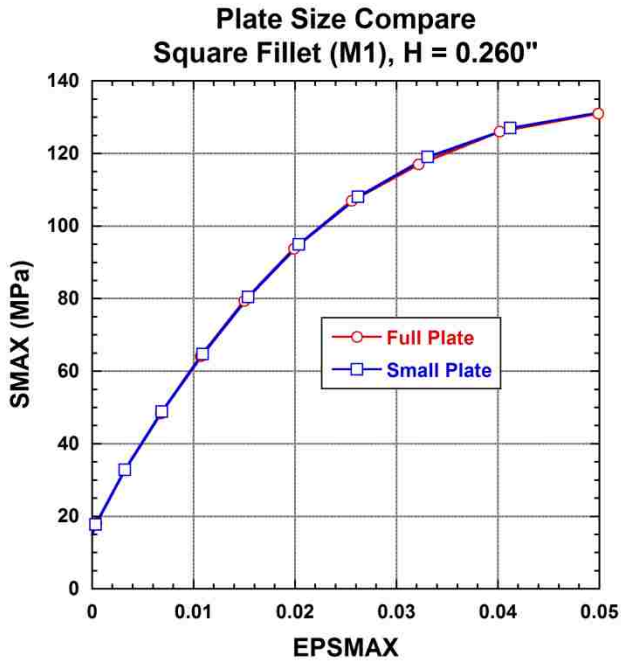

Figure 33 - Plate Size Comparison (SMAX vs EPSMAX)

The number of time steps required for accurate predictions was also examined. A time step refinement study was performed on the square fillet mesh refinement with the small plate geometry. Time steps were incremented two, three, and four times per second in

model simulation time. An element in the epoxy bond displaying the largest EPSMAX at the time corresponding to experimental failure occurred in the same element for all three time steps refinements. Plots for time step refinement displaying EPSMAX vs. Load and SMAX vs. EPSMAX of that element can be seen in Figure 34 and Figure 35. It can be seen that even doubling the number of time steps does not change the solution. Analyses for all bond geometries will use two time steps taken every second to save on computational time.

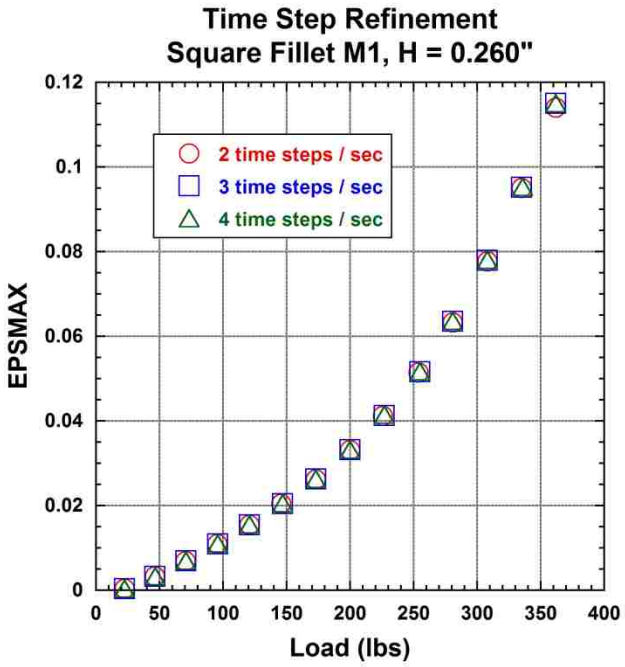

Figure 34 - Time Step Refinement for Square Fillet (EPSMAX vs Load)

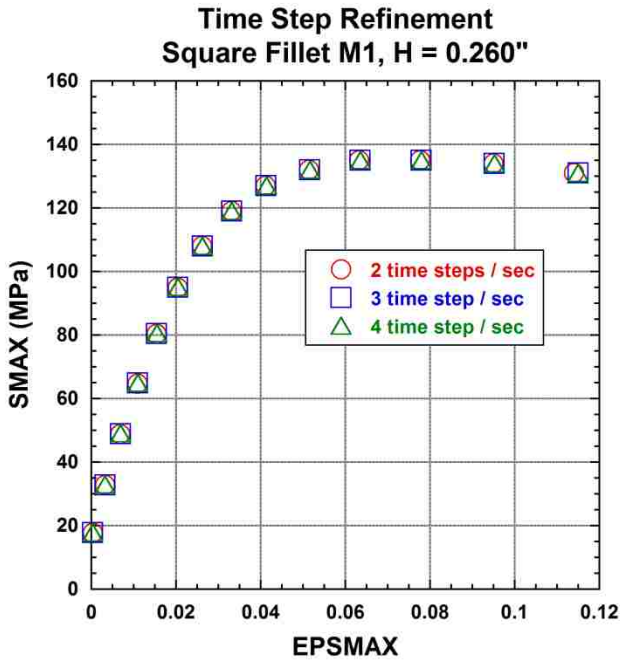

Figure 35 - Time Step Refinement for Square Fillet (SMAX vs EPSMAX)

Now that model simplifications have been determined to have negligible effect on computational predictions, spatial convergence of the square fillet can now be examined. Mesh refinements for spatial convergence analyses of the square fillet geometry are seen in Figure 36. Mesh refinement M2 is approximately ½ the size of M1 and M3 is approximately ¼ the size of M1 near the area of predicted failure. Painted element EPSMAX predictions for the square fillet epoxy bond geometry are seen in Figure 37. In each refinement of the epoxy bond, the element with the largest value of EPSMAX is at the plate interface (bottom right corner) contrary to experimental results showing failure occurring at the cylinder interface. The painted plots also show a large strain gradient at the lower right corner. Plots of EPSMAX vs. Load and SMAX vs. EPSMAX for the element at the bottom right corner of the underfill are seen in Figure 38 and Figure 39. The EPSMAX vs. Load plot shows an increasing deviation of the predictions while the SMAX vs. EPSMAX plot shows convergence with each mesh refinement. It would seem

that stress and strain with respect to each other are unaffected by mesh refinement, but examining strain against load illustrates that strain (and its respective stress) is increasing more quickly at any predicted load with each refinement. Finer meshes are sampling results closer to the corner. The lack of convergence in this respect along with a large strain gradient seen in the painted plots leads one to believe an elastic singularity (high strain gradient) exists. Elastic stress-strain singularities are not uncommon on geometries with an infinitely sharp corner. In reality, every visibly sharp corner has a finite radius, but is often neglected in FEA to simplify model creation. Although the square fillet geometry is the simplest case for an engineer to examine, the lack of spatial convergence makes this model questionable for failure predictions.

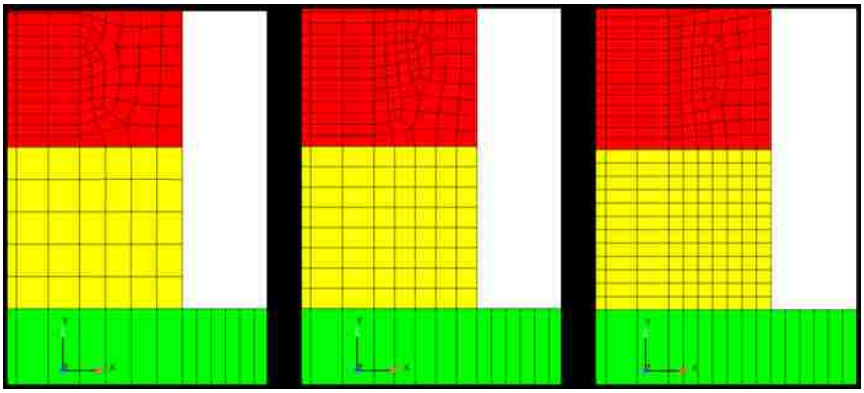

Figure 36 - Square Fillet Mesh Refinement (M1, M2, M3)

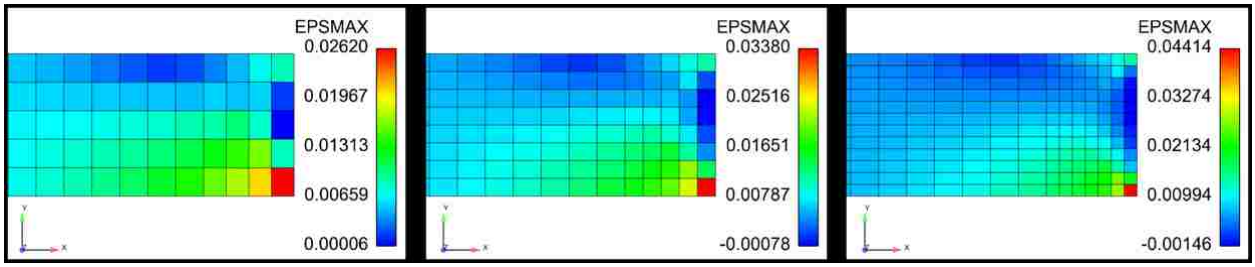

Figure 37 - Square Fillet EPSMAX Predictions for H = 0.260" (M1, M2, M3)

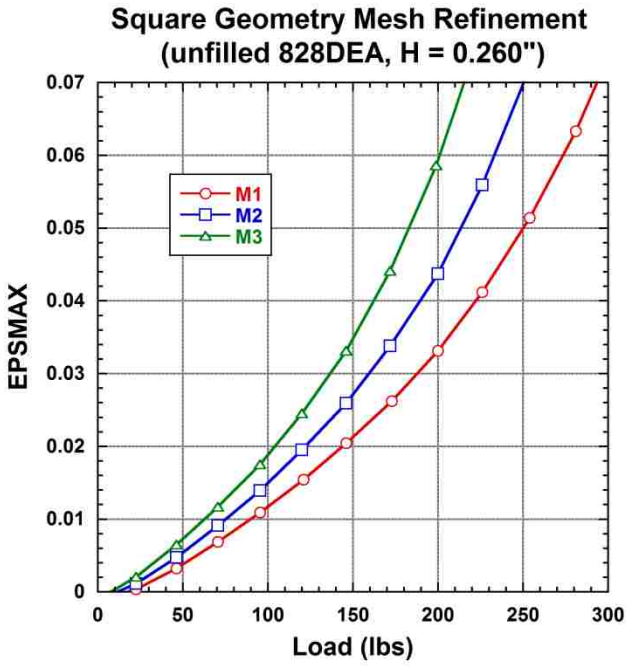

Figure 38 - Square Fillet Mesh Refinement (EPSMAX vs. Load)

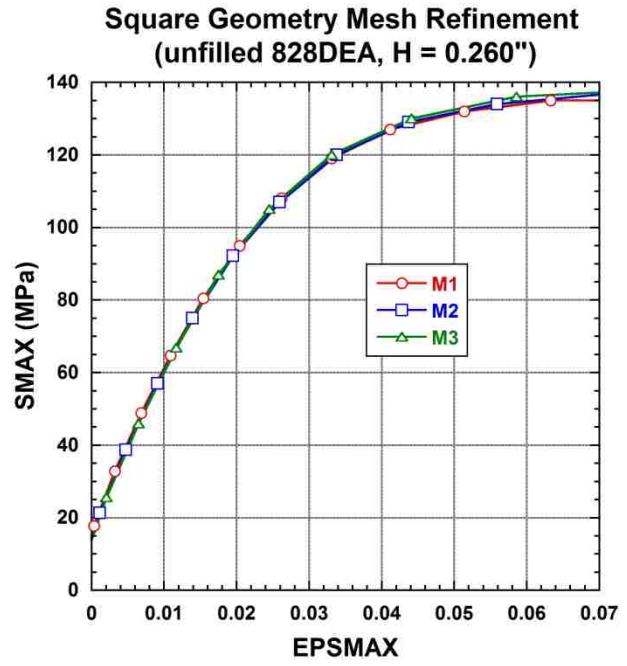

Figure 39 - Square Fillet Mesh Refinement (SMAX vs. EPSMAX)

5.1.2. Undercut fillet

The undercut fillet idealizes a situation in which there is no wetting and an exaggerated amount of volume shrinkage during cure and cool down causes the epoxy bond to pull

inward. Volume shrinkage is calculated by the SPEC model during cool down, but the magnitude of the shrinkage is quite small. The undercut model exaggerates that effect to examine a hypothetical meniscus geometry. Undercut fillet mesh refinements can be seen in Figure 40. Mesh refinement M2 is approximately ½ the size of M1 and M3 is approximately 1/5 the size of M1 near the area of predicted failure. Painted element EPSMAX predictions for the undercut geometry can be seen in Figure 41. Similar to the square fillet, refinements show that the element with the largest value of EPSMAX is at the plate interface (lower right corner). However, unlike the square fillet, the curved shape of the undercut fillet has a less extreme strain gradient at the plate interface. Plots of EPSMAX vs. Load and SMAX vs. EPSMAX for the element in the bottom right corner of the epoxy bond can be seen in Figure 42 and Figure 43. These plots show that the undercut fillet geometry seems to have spatial convergence without the need for a great deal mesh refinement (at least at the lower strains and loads). Although the undercut fillet geometry demonstrates a converged solution it does not predict the locus of failure corresponding to experimental failure.

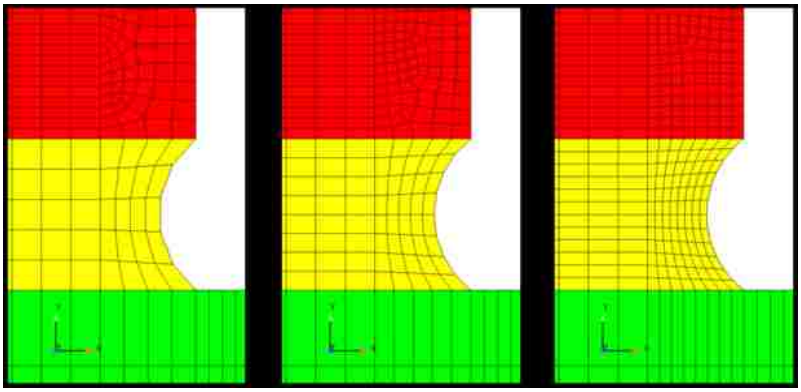

Figure 40 - Undercut Fillet Mesh Refinement (M1, M2, M3)

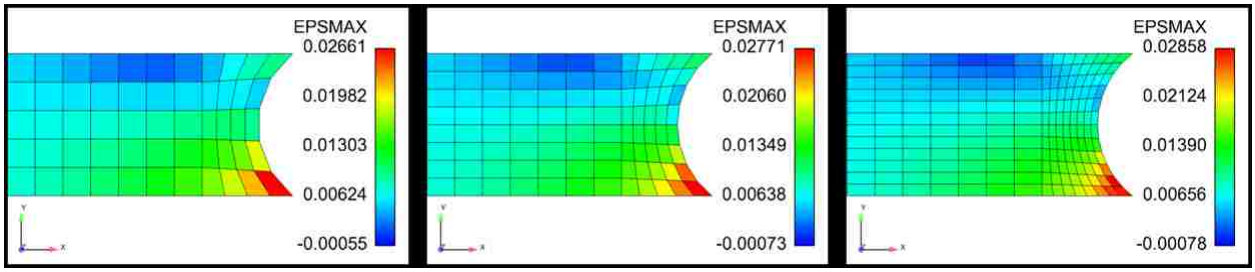

Figure 41 - Undercut Fillet EPSMAX Predictions (M1, M2, M3)

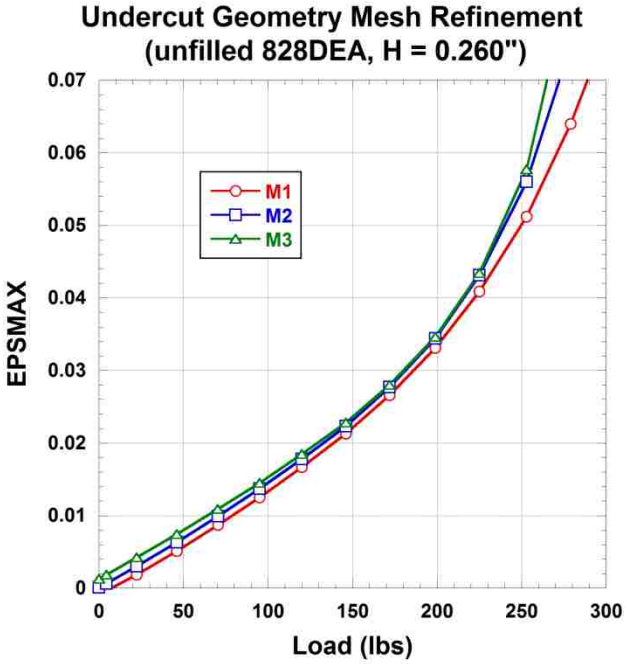

Figure 42 - Undercut Fillet Mesh Refinement (EPSMAX vs. Load)

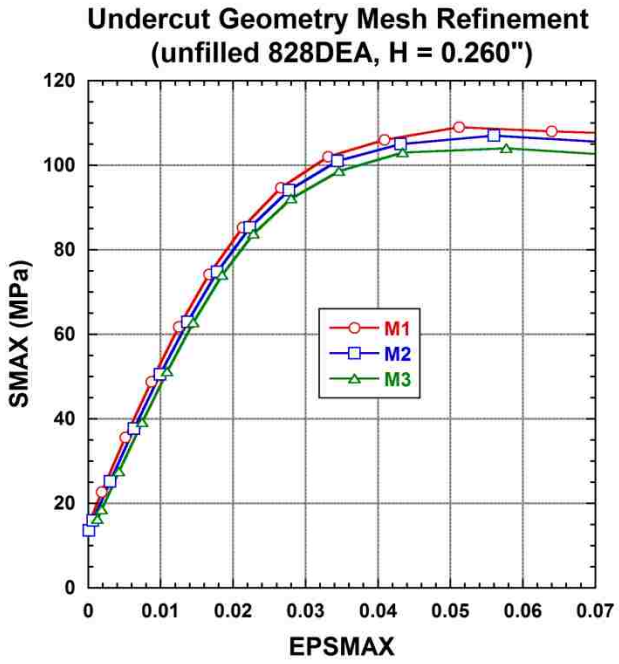

Figure 43 - Undercut Fillet Mesh Refinement (SMAX vs. EPSMAX)

5.1.3. Overflow fillet

The overflow geometry idealizes a state in which there is no epoxy wetting up the cylinder, but wetting occurs on the plate. Mesh refinements for the overflow fillet case can be seen in Figure 44. Mesh refinement M2 is approximately ½ the size of M1 and M3 is approximately ¼ the size of M1 near the area of predicted failure. Painted element EPSMAX predictions for the overflow geometry can be seen in Figure 45. The element with the largest strain in each refinement is in the top right corner of the epoxy bond. Plots of Load vs. Displacement and SMAX vs. EPSMAX for that element can be seen in Figure 46 and Figure 47. Unlike the square fillet and undercut fillet geometries, refinements show that the element with the largest value of EPSMAX is at the cylinder interface which corresponds to experimental results (top right corner of epoxy bond). However, the overflow fillet seems to suffer from the same problem as the square fillet case. Although convergence is seen on the stress-strain plot there is an increasing

deviation of the solution on the strain-load plot with each refinement. Stress and strain increase with respect to each other, but they increase more quickly at predicted loads with each mesh refinement. The large strain gradient and lack of convergence once again leads to the conclusion of an elastic singularity at the element of interest. Although the overflow fillet is the only idealized geometry that resembles the actual geometry of the epoxy bond in the test coupons, the singularity makes predictions problematic. Spatial convergence near the corner is most likely unobtainable.

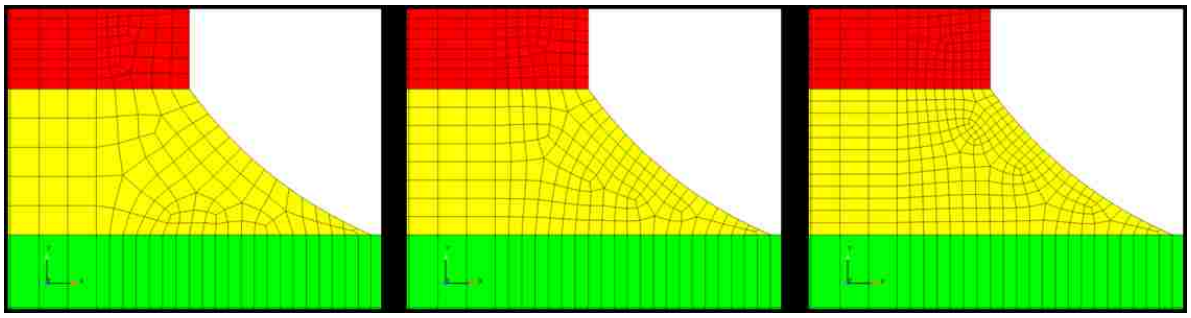

Figure 44 - Overflow Fillet Mesh Refinement (M1, M2, M3)

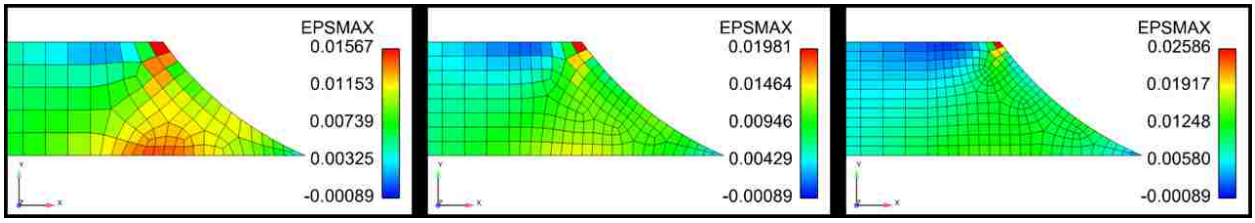

Figure 45 - Overflow Fillet EPSMAX Predictions (M1, M2, M3)

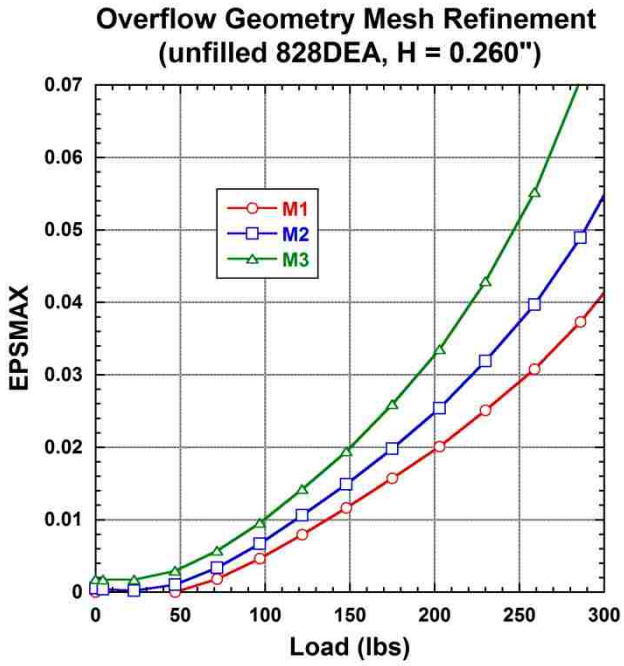

Figure 46 - Overflow Fillet Mesh Refinement (EPSMAX vs. Load)

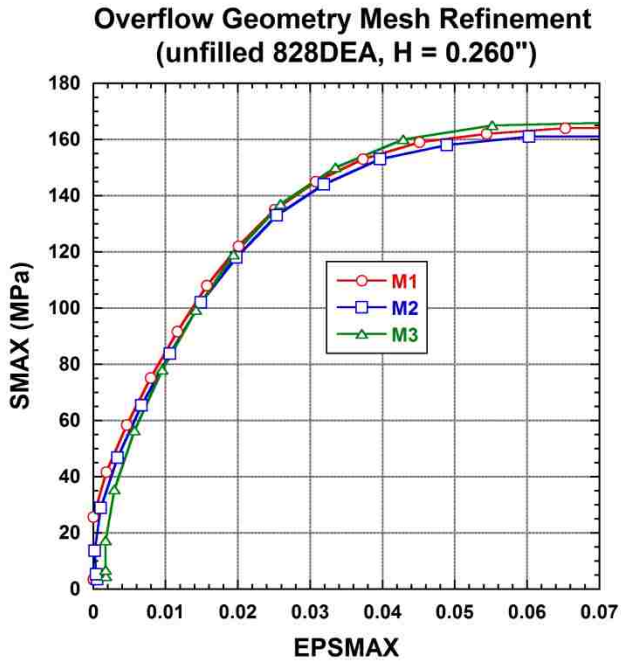

Figure 47 - Overflow Fillet Mesh Refinement (SMAX vs. EPSMAX)

5.2. Realistic epoxy bond geometry

Each of the idealized geometries are convenient and easy to create for initial engineering predictions, but do not accurately represent epoxy bond geometries seen in experimental coupons. For this reason, additional models were created to more accurately represent the cylinder chamfer and epoxy bond wetting seen in test coupons. The more realistic models can be seen in Figure 48. Mesh refinement analyses for the realistic epoxy bond geometries are performed under the same conditions as the idealized geometry mesh refinement analyses (unfilled 828DEA epoxy, H = 0.260”).

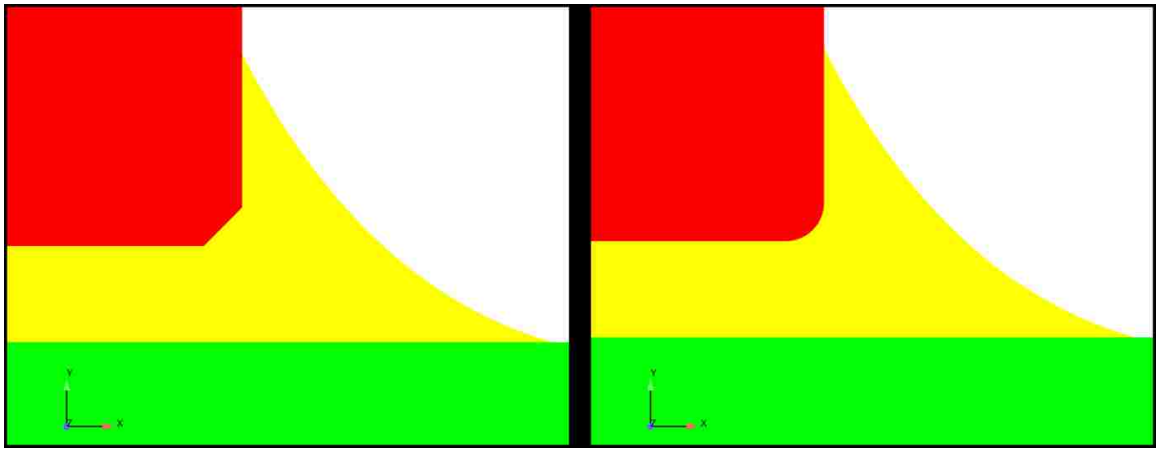

Figure 48 - Realistic Model Geometries (Chamfered and Rounded cylinder)

5.2.1. Chamfered cylinder with 0.020" wetting

The idealized overflow fillet geometry has been improved to better represent the shape of the cylinder as well as the wetting of the epoxy seen in experimental coupons. A chamfer was added to the cylinder edge as well as a 0.020" epoxy wetting on the cylinder wall which is similar to the wetting seen in the “normal” fabricated test coupons. Chamfer geometry mesh refinements can be seen in Figure 49. Mesh refinement M2 is approximately 2/5 the size of M1 and M3 is approximately 1/5 the size of M1 near the

area of predicted failure. Painted element EPSMAX predictions for the chamfer geometry can be seen in Figure 50. The painted plots show a strain concentration occurring at one of the corners of the chamfer which brings up the concern of an elastic singularity similar to what was seen in the idealized geometries. However, a plot of EPSMAX vs. Load of the element in the corner, seen in Figure 51, shows that the solution is starting to converge with each mesh refinement. A plot of SMAX vs. EPSMAX for that same element, seen in Figure 52, also displays signs of a converging solution. Although the third refinement (M3) examined may not be a completely converged mesh, there is less than a 10% difference in EPSMAX predictions at the time of failure (172 lbs) when comparing the second refinement (M2) to the third (M3). Less improvement is expected from further refinement. The chamfer geometry with wetting closely represents actual coupon geometrical features and has a reasonably converged solution.

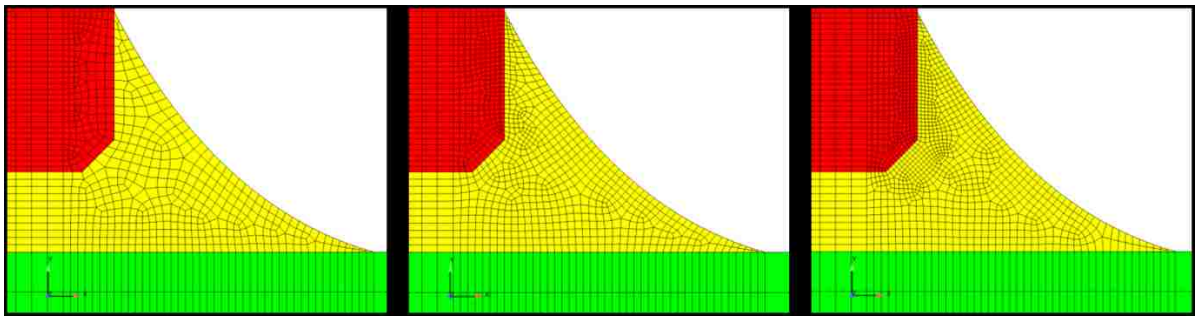

Figure 49 - Overflow w/ Chamfer Mesh Refinement with 0.020" Cylinder Wetting (M1, M2, M3)

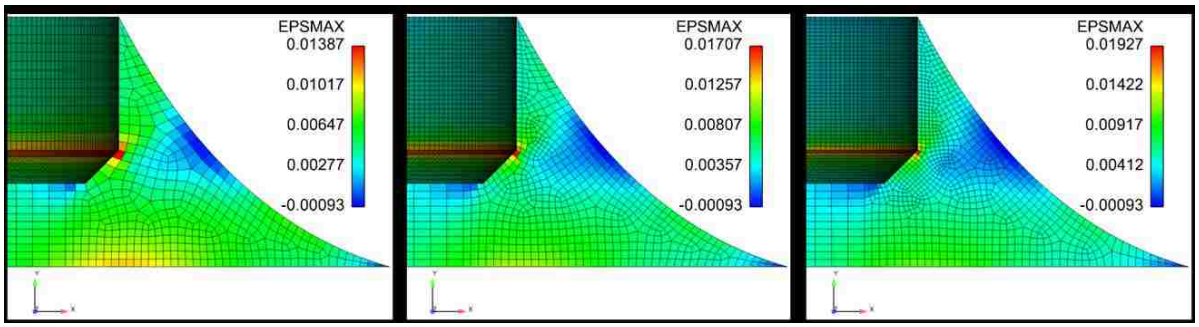

Figure 50 - Overflow w/ Chamfer and 0.020" Cylinder Wetting EPSMAX Predictions (M1, M2, M3)

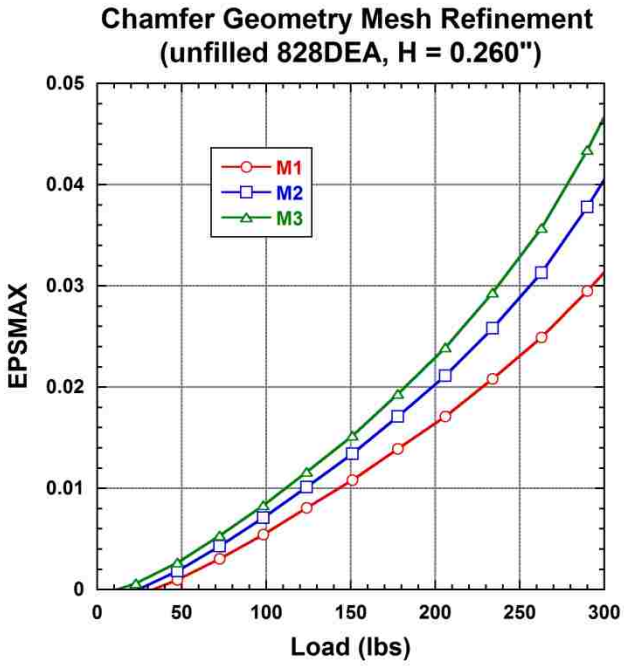

Figure 51 - Overflow w/ Chamfer and 0.020" Wetting Mesh Refinement (EPSMAX vs. Load)

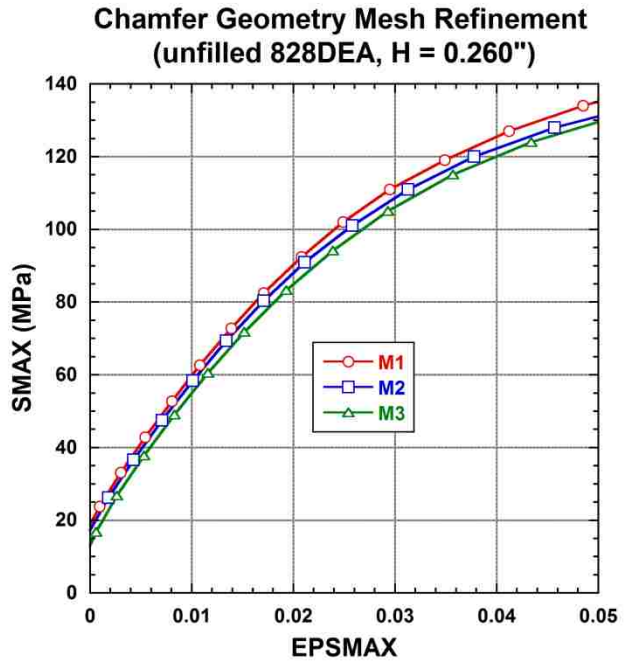

Figure 52 - Overflow w/ Chamfer and 0.020" Wetting Mesh Refinement (SMAX vs. EPSMAX)

5.2.2. Rounded cylinder with 0.020" wetting

A round cylinder geometry was also investigated for comparison to the chamfer case as was done in the experiments. Data shows negligible difference between the chamfered and rounded cylinder coupons, but a FEA comparison will determine if failure predictions remain unaffected by cylinder geometry as well. The rounded geometry has the same amount of wetting as the chamfered case and the cylinder has the same radius as the chamfer, only rounded. Mesh refinement for the chamfered geometry can be seen in Figure 53. Mesh refinement M2 is approximately ½ the size of M1 and M3 is approximately 1/5 the size of M1 near the area of predicted failure. Painted element EPSMAX predictions for the rounded geometry can be seen in Figure 54. The element with the largest EPSMAX is at the rounded portion of the cylinder interface. Plots of EPSMAX vs. Load and SMAX vs. EPSMAX can be seen in Figure 55 and Figure 56. Convergence of the solution for mesh refinement of the rounded cylinder is similar to that of the chamfered cylinder. When looking at the EPSMAX vs. Load plot there is less than 10% change in the solution when comparing the second refinement (M2) to the third refinement (M3). Similar results are seen in the EPSMAX vs. Stress plot. Minor improvement is expected from further refinement. The rounded cylinder geometry with wetting on the cylinder also closely represents coupon geometries and has a reasonably converged solution. The rounded cylinder geometry can also serve as an idealized version of the chamfered case to eliminate sharp corners in the model.

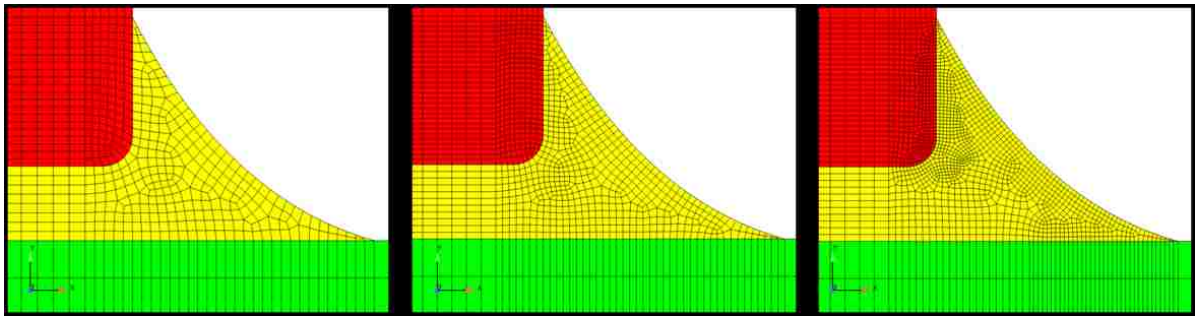

Figure 53 - Overflow w/ Round Mesh Refinement including 0.020" cylinder wetting (M1, M2, M3)

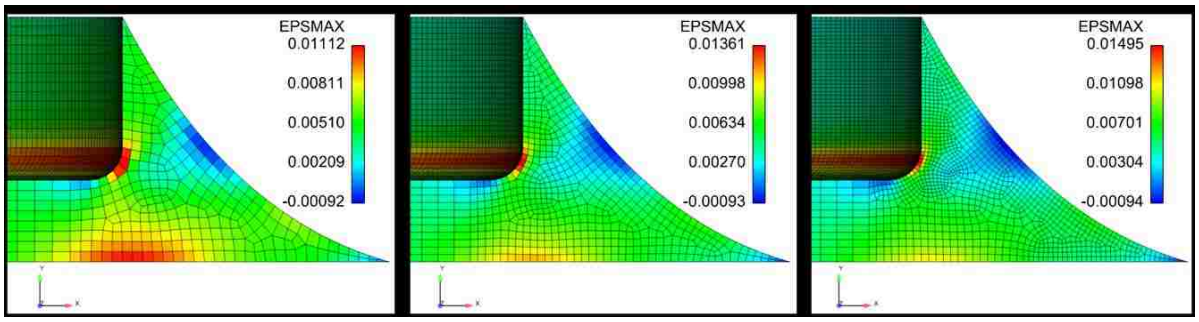

Figure 54 - Overflow w/ Round and 0.020" cylinder wetting EPSMAX Predictions (M1, M2, M3)

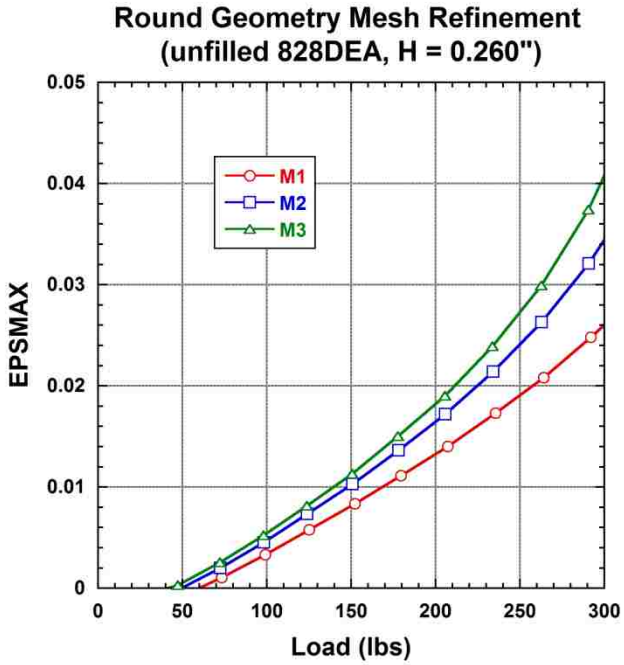

Figure 55 - Overflow w/ Round and 0.020" Wetting Mesh Refinement (EPSMAX vs. Load)

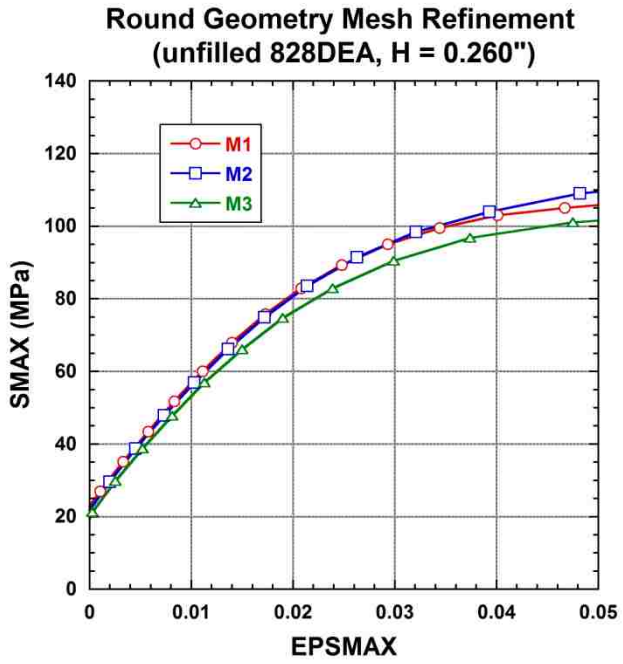

Figure 56 - Overflow w/ Round and 0.020" Wetting Mesh Refinement (SMAX vs. EPSMAX)

5.3. Model geometry discussion

Idealized geometry models are convenient for initial analyses because they are easy to create, but ultimately can suffer from elastic stress-strain singularities that cause convergence issues or inaccurate locus of failure predictions. Spatial convergence is especially sensitive to the infinitely sharp corners modeled in the idealized cases. The realistic models eliminate these issues by capturing small geometrical details found in the test coupons while eliminating infinitely sharp corners that cause stress-strain singularities. Further refinement of the realistic cases may be necessary for absolute convergence, but increasing the number of elements in the model may not be worth the modest increase in prediction accuracy. The chamfered and rounded cylinders display reasonably converged solutions and locus of failure predictions accurate with what is seen after failure of the test coupons. For these reasons, the realistic epoxy bond geometry cases will be used for the following failure predictions.

6. Failure predictions using realistic epoxy bond models

Previous analysis for cohesive and adhesive failure discussed in the literature review section determined that runaway viscoelasticity corresponded to experimental failure and that a value of EPSMAX near the onset of runaway viscoelasticity captured failure across all tests within some degree of error. Failure predictions for the following analyses will take a slightly different approach. Instead of using all available data to choose a universal value of EPSMAX, the average failure load for one pusher height will be used to determine a value of EPSMAX that will be used to predict failure for the remaining pusher heights. Knowing the value of EPSMAX that corresponds to the failure of the epoxy bond at one pusher height should allow for failure predictions of the epoxy bond at any other pusher height if EPSMAX serves as a valid failure metric. If this hypothesis is found to be true, it will establish additional support for using the EPSMAX metric as an indicator of adhesive failure initiation in glassy thermoset materials. This could translate to accurate failure predictions of epoxy underfills in electronic packages and other applications that incorporate NLVE materials.

The highest mesh refinement (M3) for realistic epoxy bond geometry models will be used for failure predictions at the five pusher heights. The chamfered and rounded case will both be investigated since the cylinder edge shape varies among the test coupons. The elements around the cylinder corner (round and chamfer) are approximately the same size making their predictions comparable to one another. This will help determine the importance of the details modeled at the cylinder corner and how those details will affect failure predictions.

6.1. Establishing an EPSMAX failure parameter

Data from the pusher height of 0.260” will be compared to the FEA predictions to establish an EPSMAX failure parameter that will be used for failure predictions of the other pusher heights. Experimental data for the pusher height of 0.260” showed an average load at failure of 172 lbs for unfilled and 202 lbs for 40vol% AlO_x 828DEA. Painted EPSMAX contour plots corresponding to a time in the analysis where the predicted load is approximately the same magnitude as the experimental load at failure can be seen in Figure 57 for the chamfered cylinder case and Figure 58 for the rounded cylinder case. The chamfered cylinder case shows the element with the largest value of EPSMAX in one of the sharp corners of the cylinder interface. The rounded cylinder case shows the element with the largest value of EPSMAX on the rounded portion of the cylinder interface.

A plot of EPSMAX vs. Load for the element with the largest value of EPSMAX in the painted plots can be seen in Figure 59 for unfilled 828DEA and Figure 60 for 40vol% AlO_x 828DEA. In both plots, a black dotted line represents the average experimental load at failure. The red and blue dotted lines show the EPSMAX value corresponding to the average experimental load at failure for the chamfer and rounded plug models. Values of EPSMAX corresponding to the average failure load as well as EPSMAX corresponding to a load one standard deviation above and below the average failure load can be seen in Table 6. Having a value of EPSMAX corresponding to the bounds of the experimental data will help develop predictions with bounds that will be used as a failure criteria for the other pusher heights. It should be noted that the EPSMAX values must be interpolated since outputted data points from the predictions did not correspond exactly to

the experimental load at failure. However, the curves from which the predictions are extracted are fairly linear making interpolation work as a reasonable approximation.

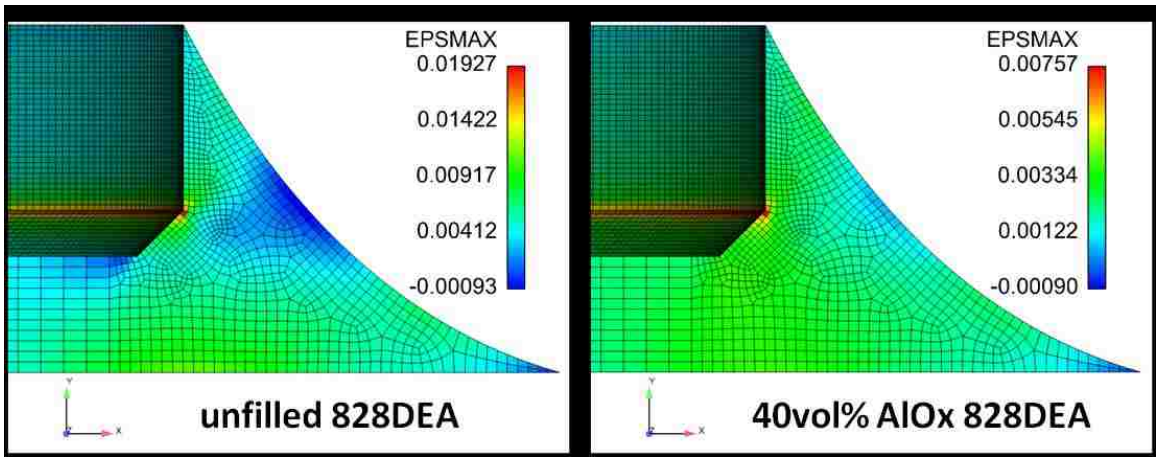

Figure 57 - EPSMAX near predicted failure load for chamfer cylinder at H = 0.260"

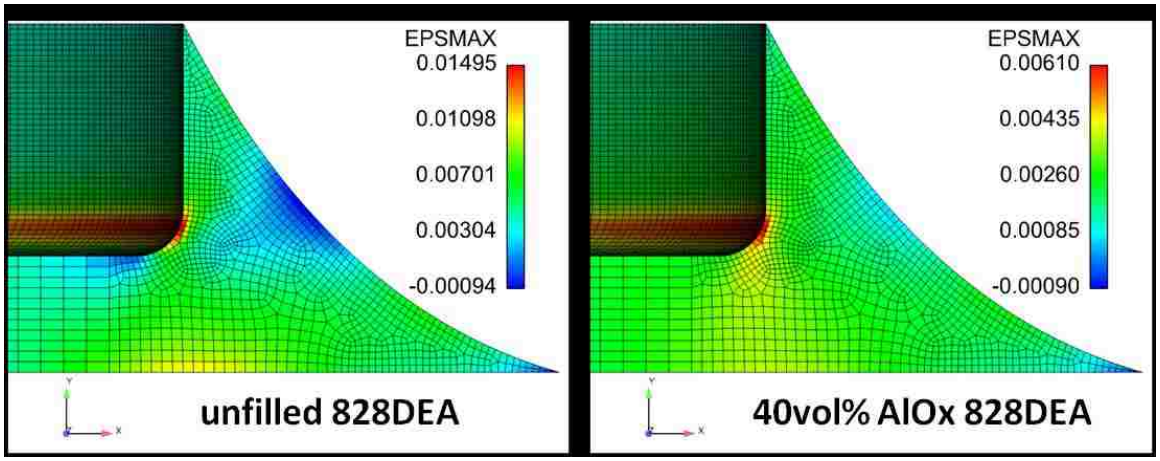

Figure 58 - EPSMAX near predicted failure load for round cylinder at H = 0.260"

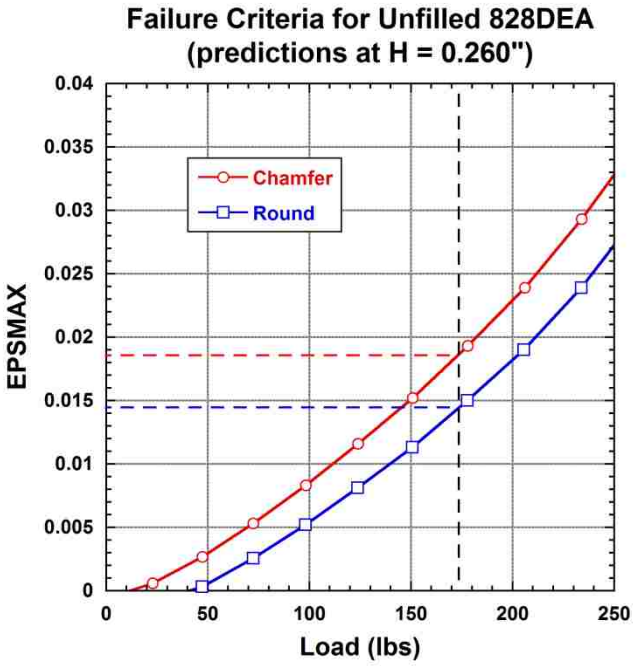

Figure 59 - Failure Criteria for Unfilled 828DEA

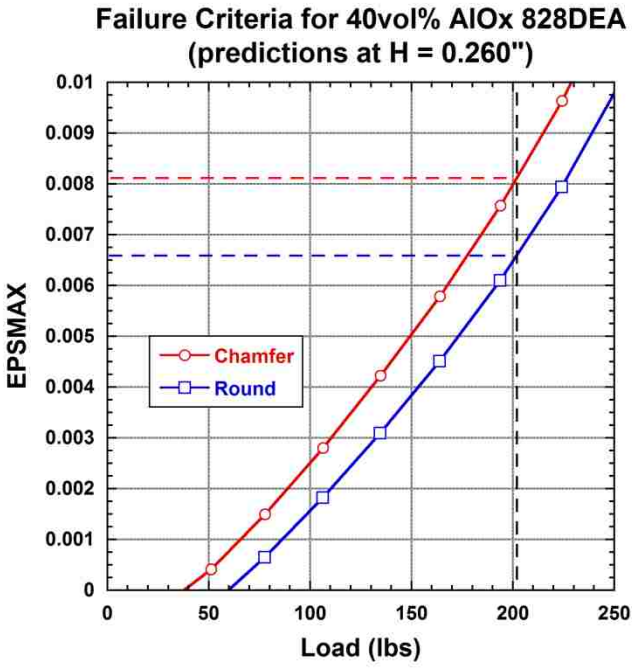

Figure 60 - Failure Criteria for 40vol% AlO_x 828DEA

Table 6 - EPSMAX Failure Parameter Based on H = 0.260"

	Unfilled EPSMAX Predicted Failure Parameter			40vol% AlO_x EPSMAX Predicted Failure Parameter		
	Min	Avg	Max	Min	Avg	Max
EPSMAX (chamfer)	0.0141	0.0185	0.0234	0.0058	0.0081	0.0108
EPSMAX (rounded)	0.0104	0.0142	0.0186	0.0045	0.0066	0.0090

6.2. Results for failure predictions of chamfer and rounded cylinder

Values of EPSMAX gathered from the pusher height of 0.260" were then used for predicted failure loads of the other four pusher heights. Painted EPSMAX contour plots for the pusher heights of 0.025”, 0.105”, 0.180”, and 0.374” at the predicted load corresponding closely to experimental failure can be seen in Figure 61 through Figure 64 for the chamfer cylinder case. The failure site for the lowest pusher height (0.025”) is at the lower corner of the chamfer while the failure site at the other pusher heights is at the upper corner of the chamfer. A plot of EPSMAX vs. Load and SMAX vs. EPSMAX for the element with the largest value of EPSMAX in the chamfer painted plots can be seen in Figure 65 and Figure 66 for unfilled 828DEA. Similar plots for 40vol% AlO_x 828DEA can be seen in Figure 67 and Figure 68. In all of the plots, a black dotted line represents EPSMAX corresponding to the average failure load at H = 0.260". The green bar extends to the upper and lower bounds of the EPSMAX failure criteria established at H = 0.260”. The SMAX vs. EPSMAX plots are created to determine if the element being examined has yielded, characteristic of runaway viscoelasticity. Presumably, the EPSMAX failure criterion should correspond somewhere close to the time the stress-strain curve "bends" or becomes nonlinear. All failure load predictions for each pusher height that fall within

the green bar in the EPSMAX vs. Load plots are recorded in Table 7 for the chamfer cylinder case. Comparison of the predicted load at failure for the chamfer model to the experimental data can be seen in Figure 69 for unfilled 828DEA and Figure 70 for 40vol% AlO_x 828DEA.

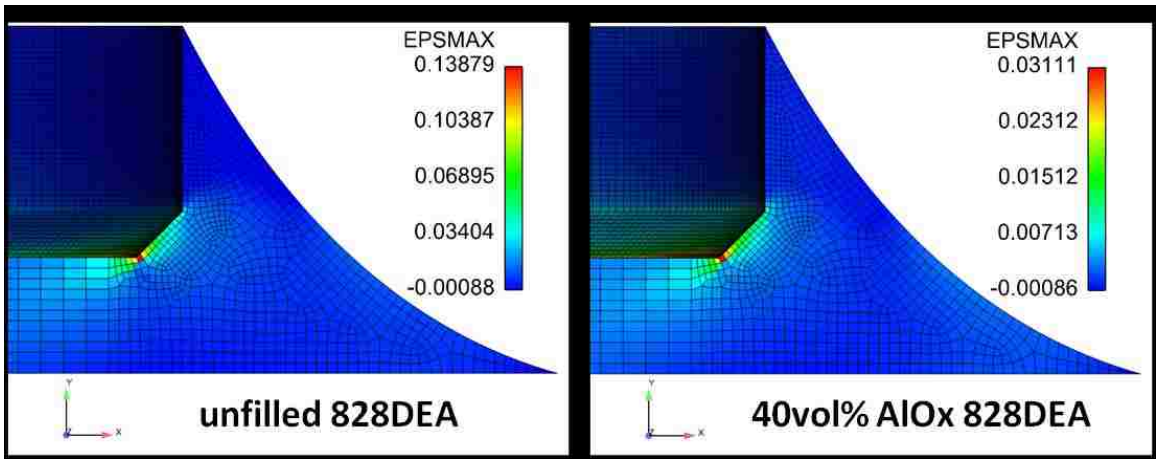

Figure 61 - EPSMAX near predicted failure load for chamfer cylinder at H = 0.025"

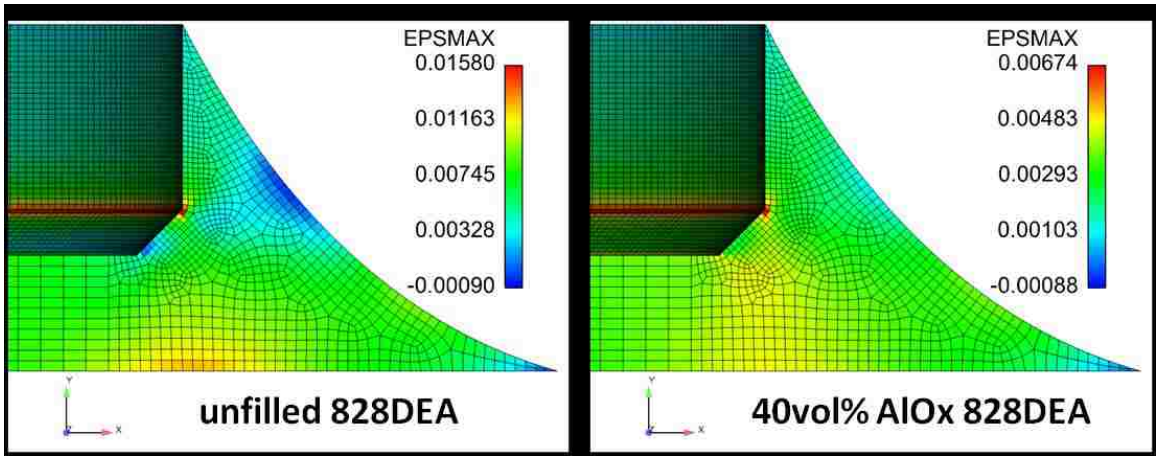

Figure 62 - EPSMAX near predicted failure load for chamfer cylinder at H = 0.105”

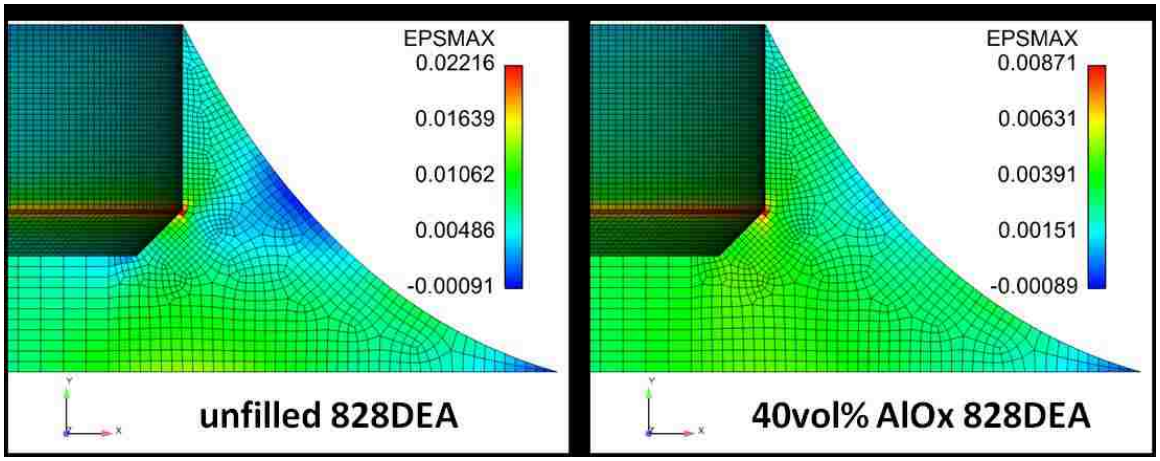

Figure 63 - EPSMAX near predicted failure load for chamfer cylinder at H = 0.180"

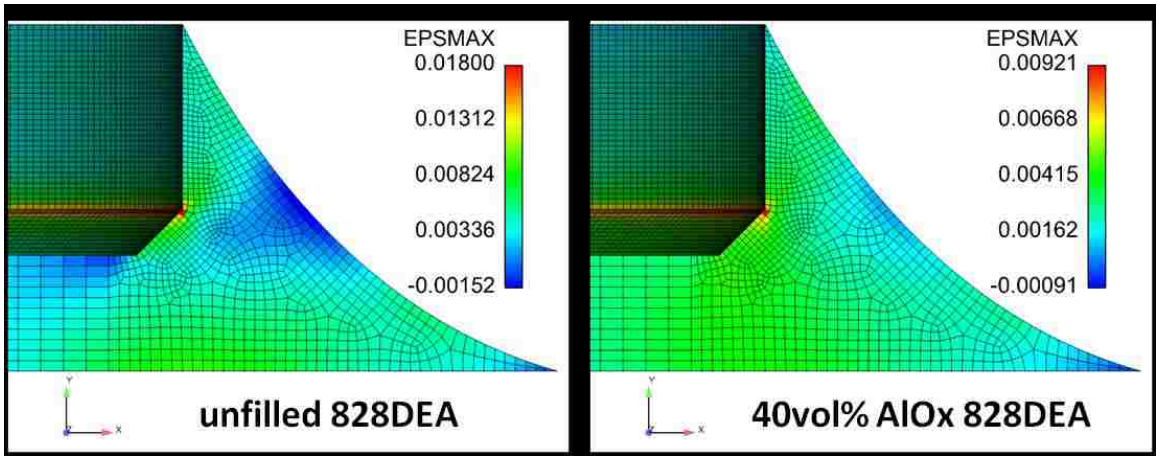

Figure 64 - EPSMAX near predicted failure load for chamfer cylinder at H = 0.374"

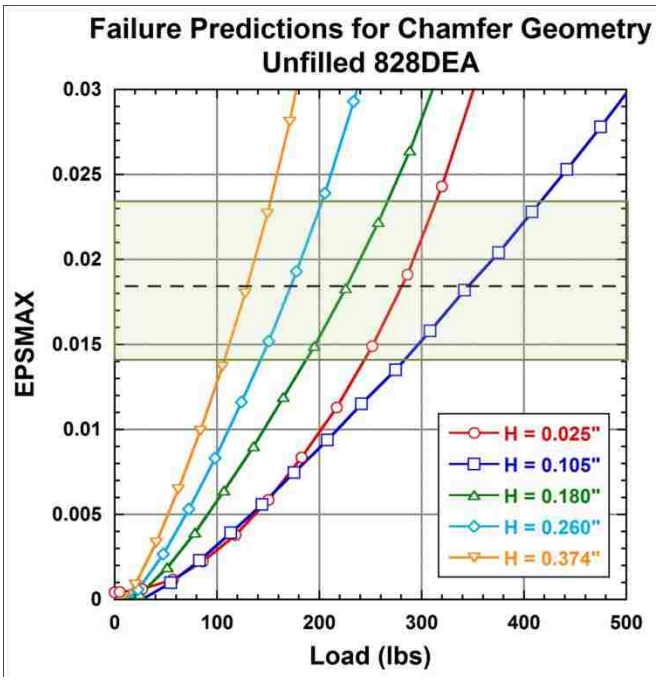

Figure 65 - EPSMAX vs. Load for Unfilled 828DEA (Chamfer Geometry)

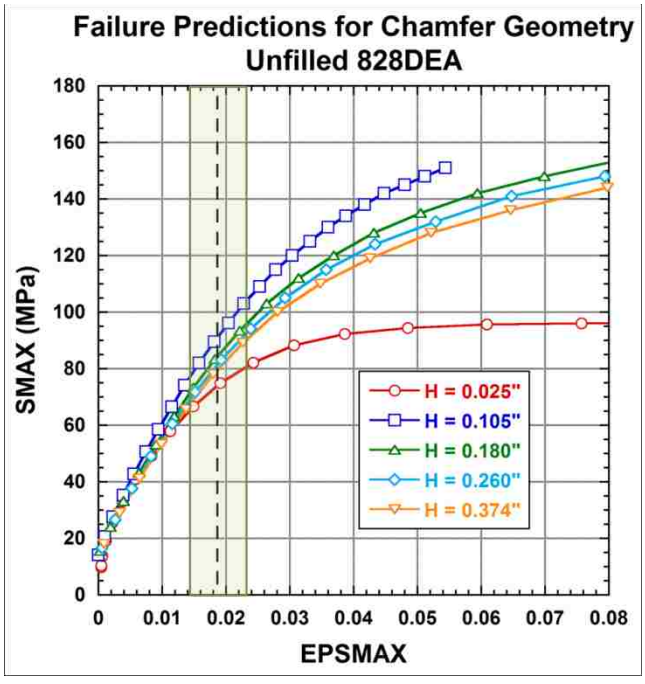

Figure 66 - SMAX vs. EPSMAX for Unfilled 828DEA (Chamfer Geometry)

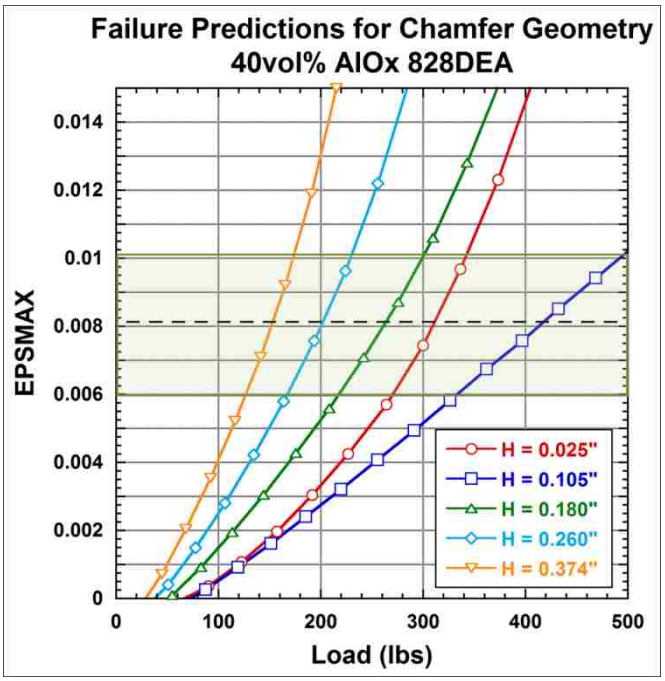

Figure 67 - EPSMAX vs. Load for 40vol% AlO_x 828DEA (Chamfer Geometry)

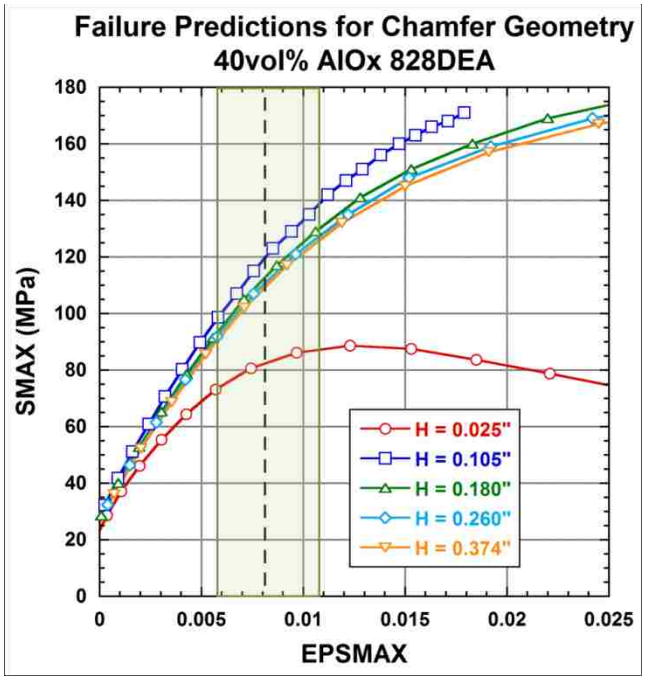

Figure 68 - SMAX vs. EPSMAX for 40vol% AlO_x 828DEA (Chamfer Geometry)

Table 7 - Predicted Failure Load Based on H = 0.260" EPSMAX Parameter (chamfer cylinder)

Pusher Height (in)	Unfilled Predicted Load at Failure (lbs)			40vol% AlO_x Predicted Load at Failure (lbs)		
	Min (lbs)	Avg (lbs)	Max (lbs)	Min (lbs)	Avg (lbs)	Max (lbs)
0.025	244.53	281.36	313.62	266.88	311.02	352.90
0.105	283.78	346.80	416.14	326.42	417.78	526.18
0.180	187.32	227.06	266.64	213.79	263.59	313.10
0.260	142.67	172.53	202.39	164.53	202.00	239.49
0.374	107.27	129.84	152.20	124.37	152.95	181.28

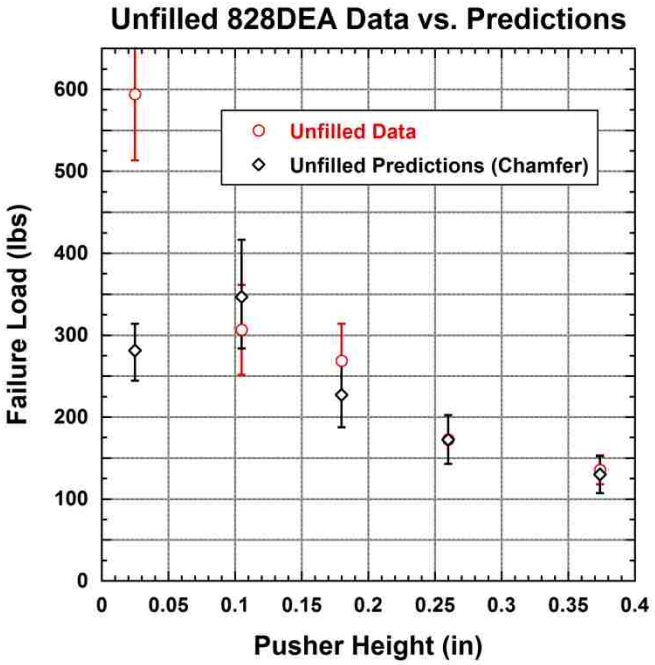

Figure 69 - Unfilled 828DEA Failure Predictions Using Chamfer Geometry

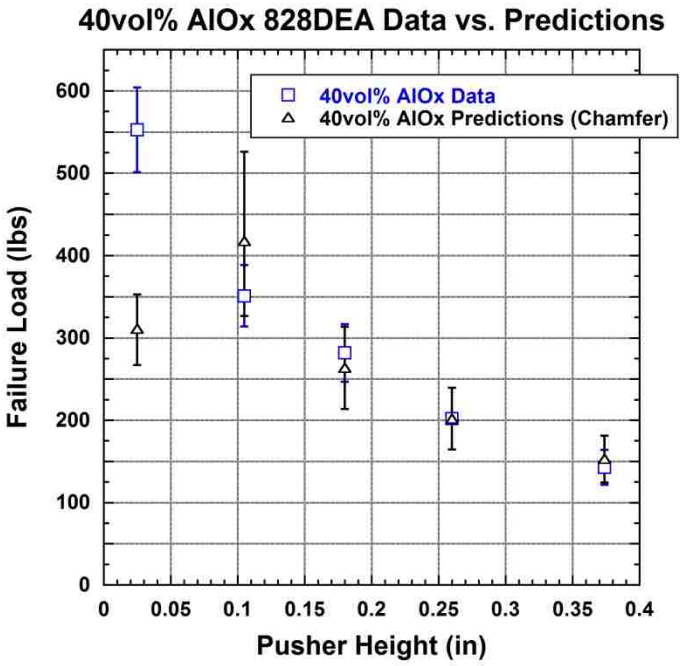

Figure 70 - 40vol% AlO_x 828DEA Failure Predictions Using Chamfer Geometry

The EPSMAX failure criteria determined from the pusher height of 0.260" was also used for failure predictions of rounded cylinder case. Painted EPSMAX contour plots of the rounded cylinder model for pusher heights of 0.025", 0.105", 0.180", and 0.374" can be seen in Figure 71 through Figure 74. It should be noted from the painted plots that the unfilled epoxy bond at a pusher height of 0.105" is the only case in which the locus of failure is not at the cylinder interface. Instead, it is predicted at the plate interface. Plots of EPSMAX vs. Load and SMAX vs. EPSMAX can be seen in Figure 75 and Figure 76 for unfilled 828DEA. The same plots for 40vol% AlO_x 828DEA can be seen in Figure 77 and Figure 78. As in the chamfer plots, the black dotted line corresponds to the average failure load EPSMAX criteria while the green box extends to the upper and lower bounds of the EPSMAX criteria. All failure load predictions for each pusher height that fall within the green bar in the EPSMAX vs. Load plots are recorded in Table 8 for the rounded cylinder case. Comparison of the predicted load at failure for the rounded

cylinder model to the experimental data can be seen in Figure 79 for unfilled 828DEA and Figure 80 for 40vol% AlO_x 828DEA.

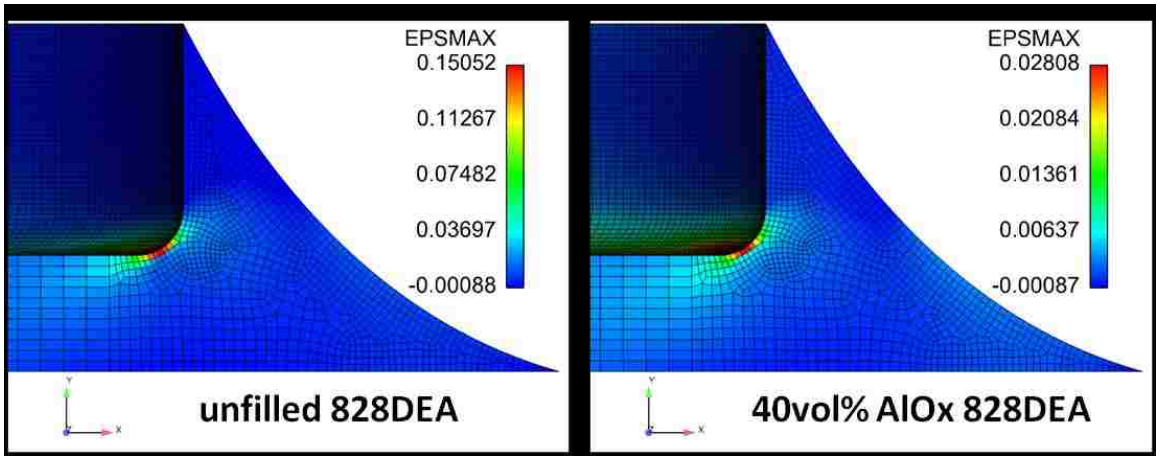

Figure 71 – EPSMAX near predicted failure load for round cylinder at H = 0.025"

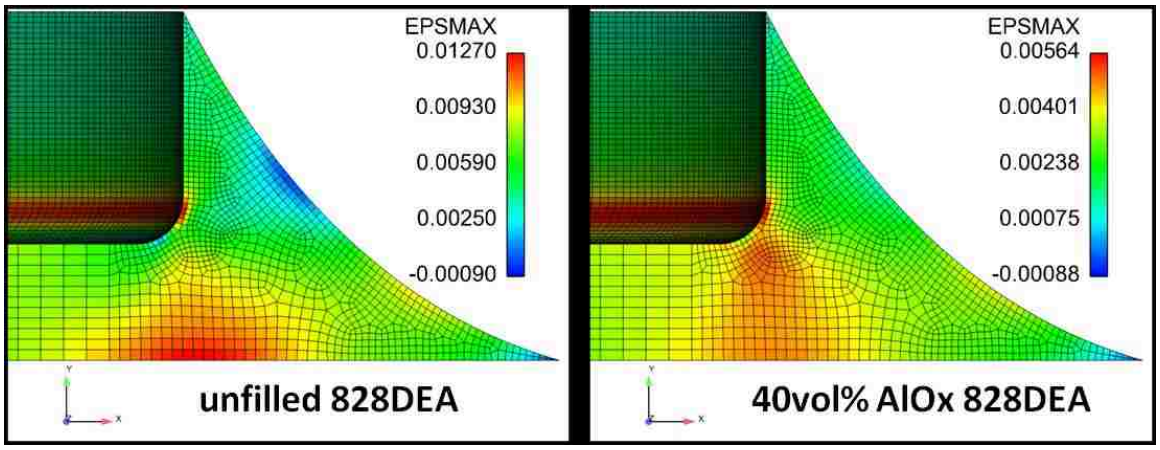

Figure 72 - EPSMAX near predicted failure load for round cylinder at H = 0.105"

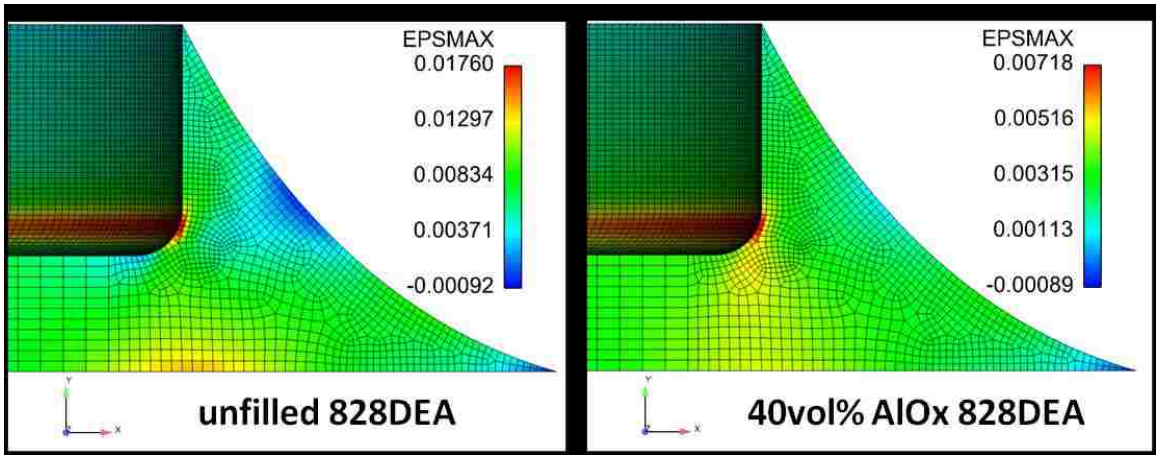

Figure 73 - EPSMAX near predicted failure load for round cylinder at H = 0.180"

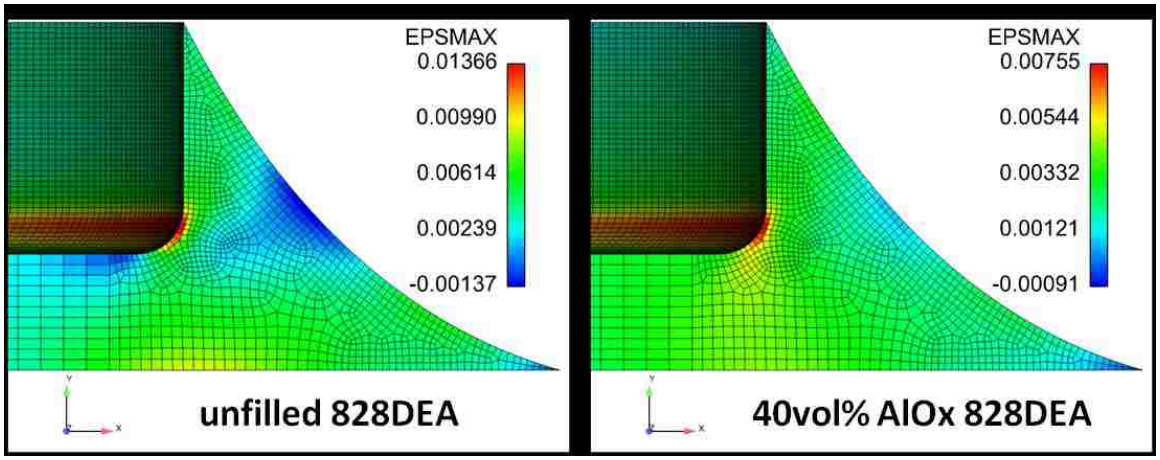

Figure 74 - EPSMAX near predicted failure load for round cylinder at H = 0.374"

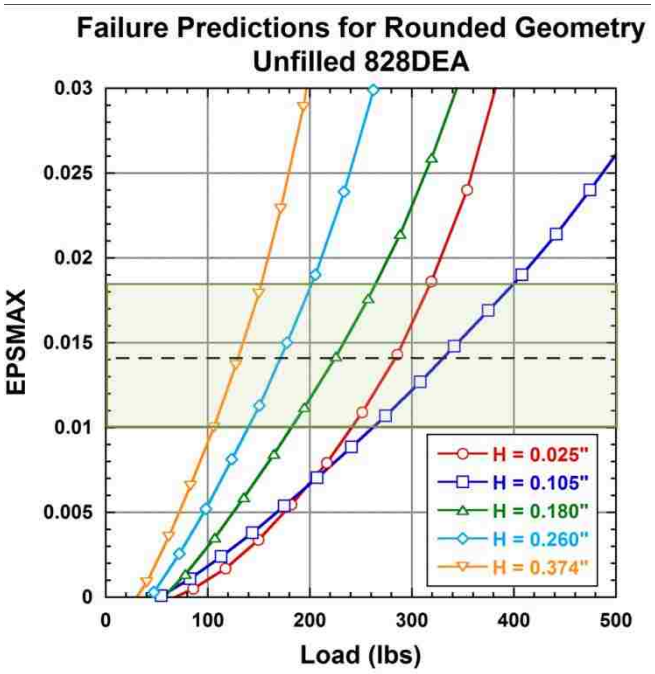

Figure 75 - EPSMAX vs. Load for Unfilled 828DEA (Rounded Geometry)

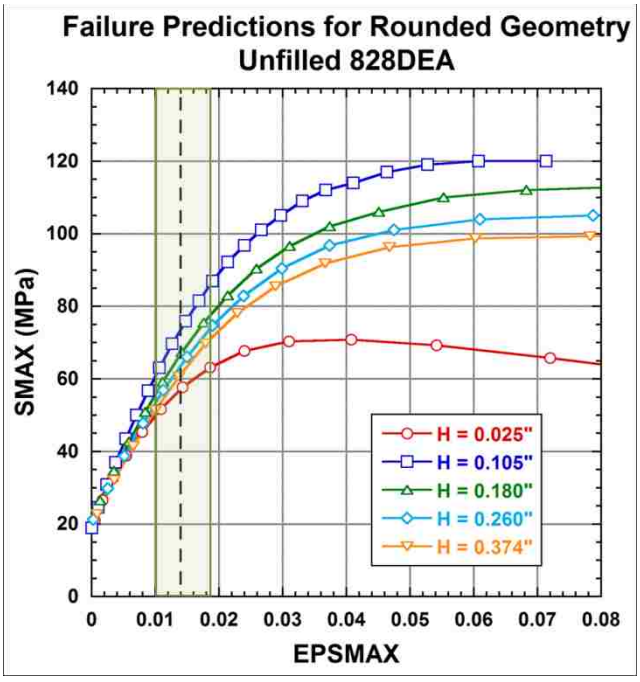

Figure 76 - SMAX vs. EPSMAX for Unfilled 828DEA (Rounded Geometry)

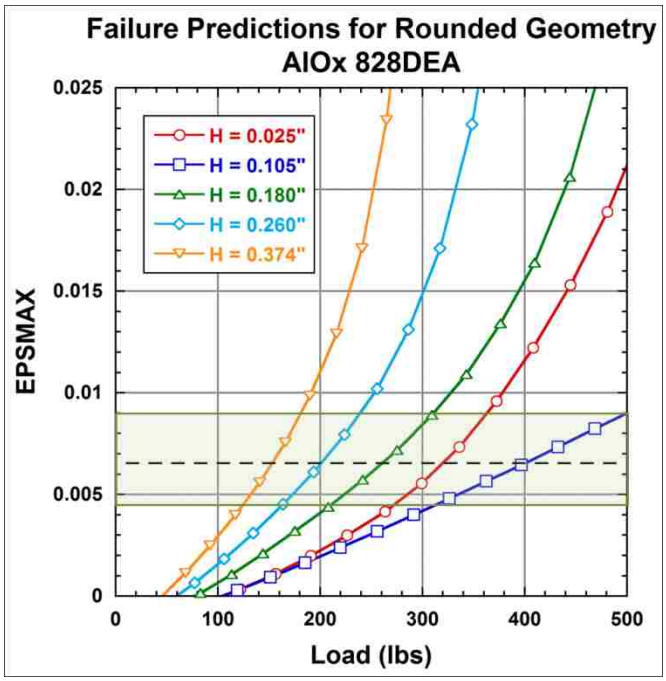

Figure 77 - EPSMAX vs. Load for AlO_x 828DEA (Rounded Geometry)

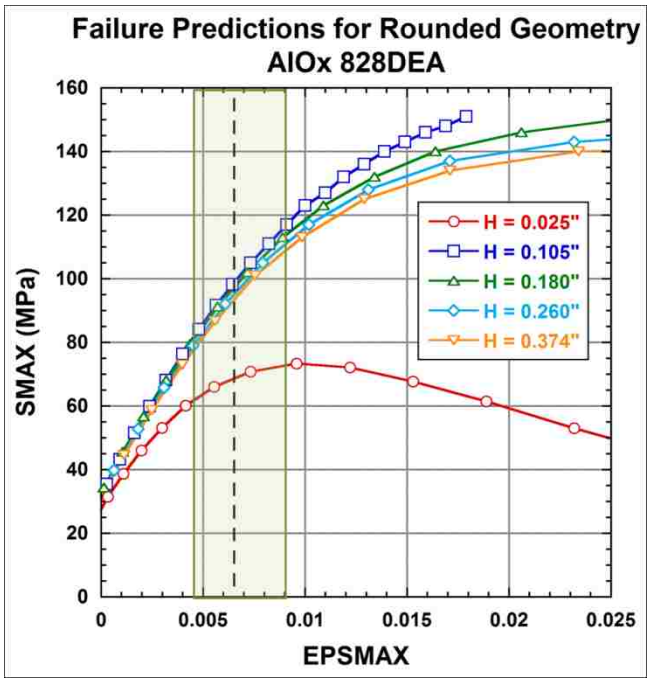

Figure 78 - SMAX vs. EPSMAX for AlO_x 828DEA (Rounded Geometry)

Table 8 - Predicted Failure Load Based on H = 0.260" EPSMAX Parameter (rounded cylinder)

Pusher Height (in)	Unfilled Predicted Load at Failure (lbs)			40vol% AlO_x Predicted Load at Failure (lbs)		
	Min (lbs)	Avg (lbs)	Max (lbs)	Min (lbs)	Avg (lbs)	Max (lbs)
0.025	245.62	285.30	319.03	273.50	321.02	363.89
0.105	268.51	333.28	400.54	315.43	403.02	501.73
0.180	186.22	226.14	265.41	212.03	261.91	311.52
0.260	142.67	172.53	202.39	164.53	202.00	239.49
0.374	107.89	130.70	152.83	125.42	153.82	181.87

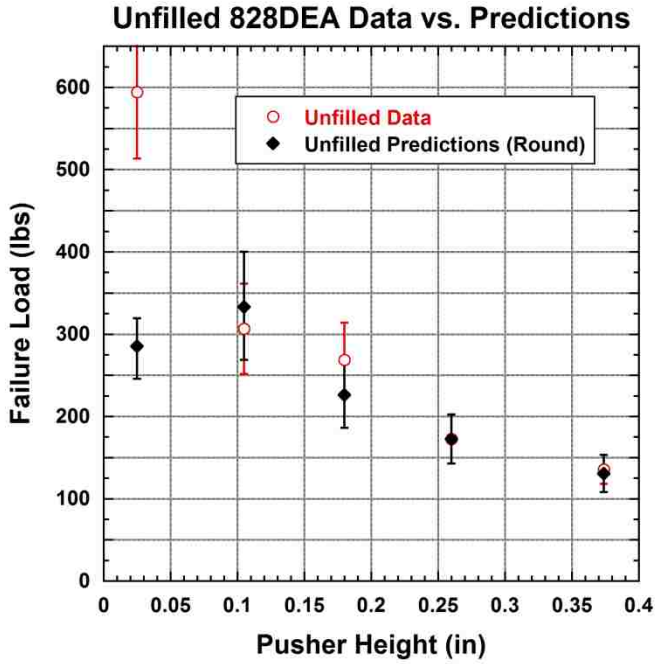

Figure 79 - Unfilled 828DEA Failure Predictions Using Rounded Geometry

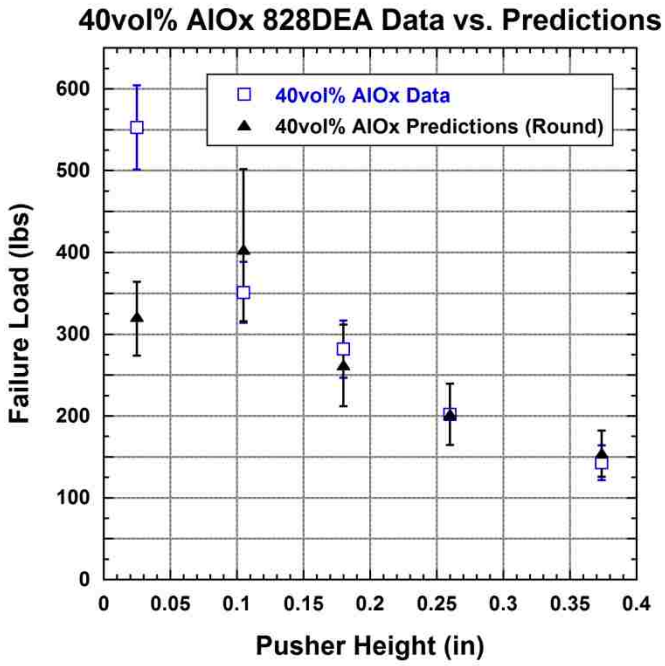

Figure 80 - 40vol% AlO_x 828DEA Failure Predictions Using Rounded Geometry

It is interesting to see that chamfered and rounded cylinder geometries predict similar failure loads for the epoxy bond at all pusher heights for unfilled and AlO_x filled 828DEA. Additionally, the failure predictions for pusher heights of 0.105", 0.180", and 0.374" match the data closely within the standard deviation of the data and predictions. The predicted load for H = 0.260" matches perfectly for both the chamfer and rounded geometries since that pusher height was used for the failure parameter. However, the predicted failure load for the pusher height of 0.025" is much lower than the experimental data. When examining the predictions for the other four pusher heights a noticeable trend can be seen where the predicted failure load increases with a decrease in pusher height. That trend deviates at the lowest pusher height where one would anticipate a continual increase in failure load with a decrease in pusher height just as is seen in the data.

When examining the epoxy bond at the lowest pusher height (H = 0.025") it is immediately noticeable from the painted element plots that EPSMAX is much higher at

the time of experimental failure than other pusher heights. In the EPSMAX vs. Load plot, the curves follow a trend where EPSMAX increases more quickly at any given load as the pusher height is increased (Figure 75 and 77). This would explain why the established EPSMAX failure parameter is reached at smaller loads as the pusher height is increased. The lowest pusher height seems to defy this trend by predicting failure somewhere between the pusher height of 0.105" and 0.180". When examining the SMAX vs. EPSMAX plot it is again noticed that the lowest pusher height does not follow the trend. For unfilled and 40vol% AlO_x 828DEA, the stress-strain curves for the other four pusher heights are roughly the same, but the lowest pusher height experiences a much lower stress at the time of failure (Figure 76 and 78). It is interesting to see that the EPSMAX failure parameter does not match up to the exact moment that runaway viscoelasticity occurs. Instead, the failure parameter corresponds to the onset of viscoelasticity or "pre-yield" of the material seen most noticeably in the SMAX vs. EPSMAX plots. A true visualization of runaway viscoelasticity cannot be seen in the EPSMAX vs. Load curve because runaway does not occur until a load much greater than what is shown on the plots.

The predictions at the lowest pusher height are certainly out of the ordinary considering the relatively accurate predictions at the other pusher heights. To better understand what makes the lower pusher height so different, a couple of geometry variations and the cylinder material properties were investigated.

6.3. Investigating lower pusher height predictions

It is possible that the geometry of the epoxy wetting on the cylinder and the bond thickness may play a much more important role at the lowest pusher height. To evaluate

these possibilities, two additional model sensitivity studies were performed on the rounded cylinder geometry with unfilled 828DEA epoxy. The first sensitivity study involved reducing the epoxy wetting from 0.020" to 0.005" on the cylinder wall. The second sensitivity study investigated increasing the epoxy bond thickness from 0.010" to 0.015" with a fixed 0.020" epoxy wetting on the cylinder. Finally, it was noticed that during the predicted deformation at the lowest pusher height, the zone of plastic strain in the cylinder was extending to the bond interface which was directly impacting the nonlinear viscoelastic response of the epoxy. This warranted a third sensitivity study to examine the role of plastic deformation by changing the constitutive model of the cylinder from elastic plastic power law hardening to pure elasticity. This was also examined for the round cylinder geometry for unfilled 828DEA with the original 0.010" bond thickness and 0.020" wetting. These three sensitivity studies were performed to determine whether the accuracy of the lower pusher height predictions was being degraded by poor approximations to the geometry or cylinder plasticity.

6.3.1. Reducing the epoxy wetting on the cylinder from 0.020" to 0.005"

Mesh refinement used on the 0.005" wetting is similar to the mesh refinement on the 0.020" wetting geometry. A painted EPSMAX contour plot of the rounded cylinder model with 0.005” wetting for the pusher height of 0.025" can be seen in Figure 81. The element of interest is at the cylinder interface of the epoxy bond. In addition to the analysis at the lowest pusher height, the 0.005" wetting case was also analyzed at the 0.260" pusher height to establish an EPSMAX failure parameter. The EPSMAX failure parameter was used to determine the predicted failure load for the 0.005" wetting case

and is compared to the predicted failure load for the original 0.020" wetting case and experimental data in Figure 82.

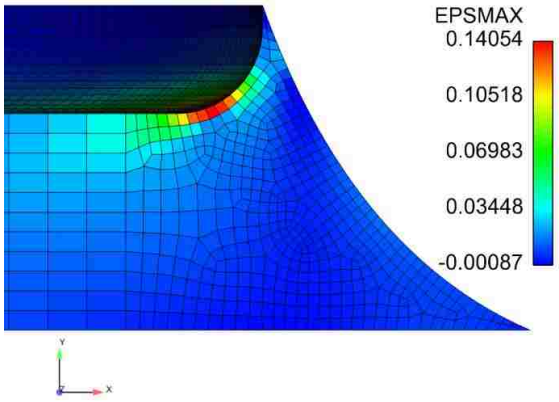

Figure 81 - EPSMAX near predicted failure load for round cylinder with 0.005" wetting at H = 0.025"

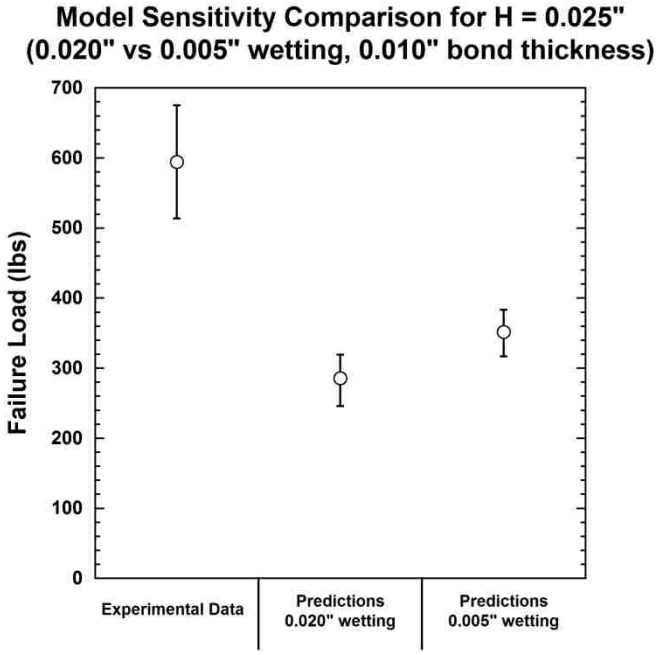

Figure 82 - Failure Load Prediction Comparing 0.020" to 0.005" Wetting at H = 0.025" (unfilled 828DEA)

The predicted average failure load for the lowest pusher height has increased from 285 lbs using the 0.020” wetting model, to 351 lbs when using the 0.005” wetting model. The predicted failure load at the lowest pusher height is still significantly lower than the

experimental data. However, the nearly 25% increase in predicted failure load is now higher than the predicted failure load for the pusher height of 0.105" with 0.020" wetting. The lowest pusher height prediction using the 0.005" wetting completes a trend with the other pusher height predictions that agrees qualitatively with the data.

6.3.2. Increasing the epoxy bond thickness from 0.010" to 0.015"

The mesh refinement used on the 0.015" epoxy bond thickness is similar to the mesh refinement on the 0.010" thickness geometry. A painted EPSMAX contour plot of the rounded cylinder model with 0.015" epoxy bond thickness for the pusher height of 0.025" can be seen in Figure 83. The element of interest is at the cylinder interface of the epoxy bond. In addition to the analysis at the lowest pusher height, the 0.015" epoxy bond thickness case was also analyzed at the 0.260" pusher height to establish an EPSMAX failure parameter. The EPSMAX failure parameter was used to determine the predicted failure load for the 0.015" epoxy bond thickness case and is compared to the predicted failure load for the original 0.010" epoxy bond thickness case and experimental data in Figure 84.

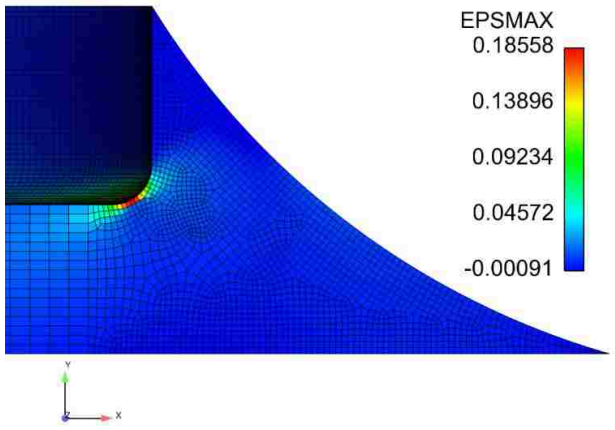

Figure 83 - EPSMAX near predicted failure load for round cylinder with 0.015" bond at H = 0.025"

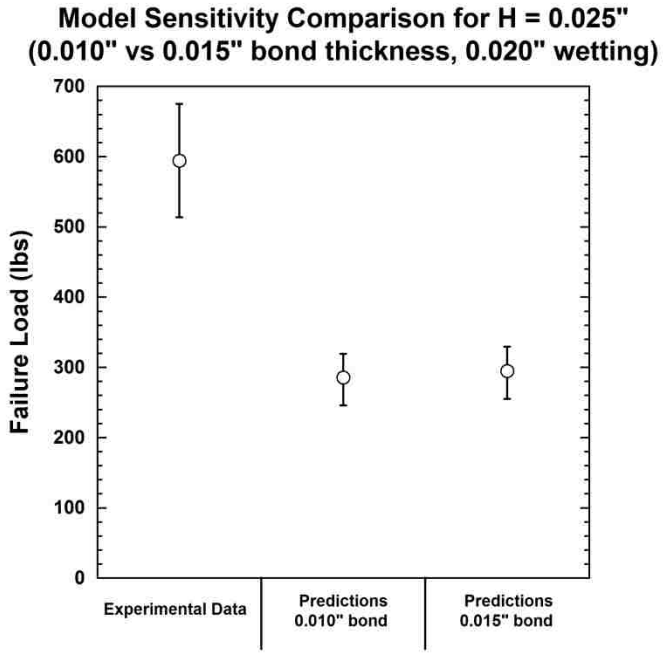

Figure 84 - Failure Load Prediction Comparing 0.015" to 0.010" Bond Thickness at H = 0.025" (unfilled 828DEA)

The predicted average failure load for the lowest pusher height has increased from 285 lbs using the 0.010" bond thickness, to 295 lbs using the 0.015" bond thickness. This small difference between predictions indicate that the model is not very sensitive to the thickness of the epoxy bond at the lowest pusher height.

6.3.3. Elastic vs. elastic plastic power law hardening model for the cylinder

The close proximity of the epoxy bond to the yielding volume of the cylinder at H = 0.025" could be affecting its stress-strain behavior during loading. A painted plot displaying equivalent plastic strain (EQPS) of the cylinder due to the contact force from the pusher when the predicted load corresponds to the experimental failure load (for H = 0.025") can be seen in Figure 85. A plastic strain in the cylinder of almost 20% is predicted to occur at the measured failure load for the 0.025"pusher height. This significant amount of strain causes material in the steel cylinder to displace downward

towards the epoxy bond. Figure 86 shows nodal displacement of the cylinder in the y-direction, with a 10x magnification of the deformation, for both the elastic plastic power law hardening cylinder model and pure elastic model (pusher has been removed from Figure 86). The magnification shows that the yield from the plasticity model is indeed causing the cylinder to displace downward, compressing the epoxy bond. The elastic model shows the material beneath the contact region of the pusher moving up instead of down. Using a pure elastic model for the cylinder will not cause a compressive effect on the epoxy bond beneath the contact region of the pusher.

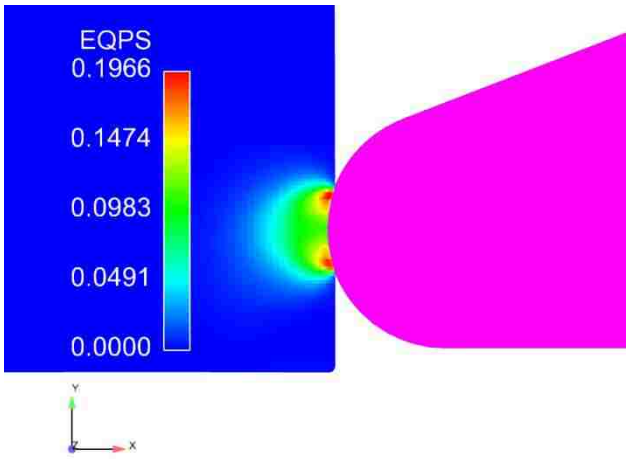

Figure 85 - Equivalent Plastic Strain (EQPS) of Cylinder at H = 0.025"

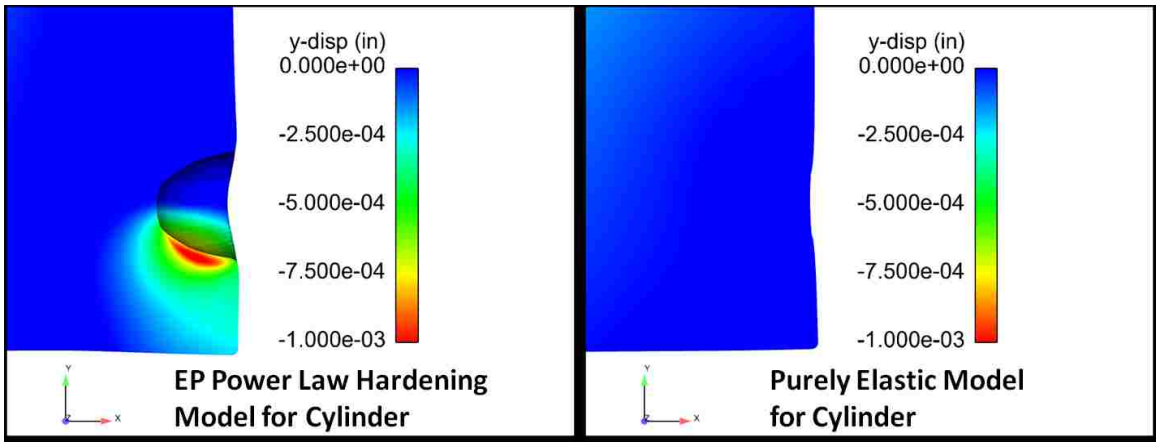

Figure 86 - Material Displacement of Cylinder (10x displacement magnification)

A comparison of painted EPSMAX contour plots for the lowest pusher height using the elastic plastic power law hardening model and elastic model (when the predicted load corresponds to the experimental failure load) can be seen in Figure 87. With the elastic model, the element displaying the largest EPSMAX at failure has moved from the cylinder interface to the plate interface, although there is still a secondary strain concentration at the cylinder interface. More importantly, the largest value of EPSMAX has dropped from 15% to 2.6% when using the elastic model for the cylinder. The EPSMAX value of 2.6% is more comparable to what is seen at the other pusher heights.

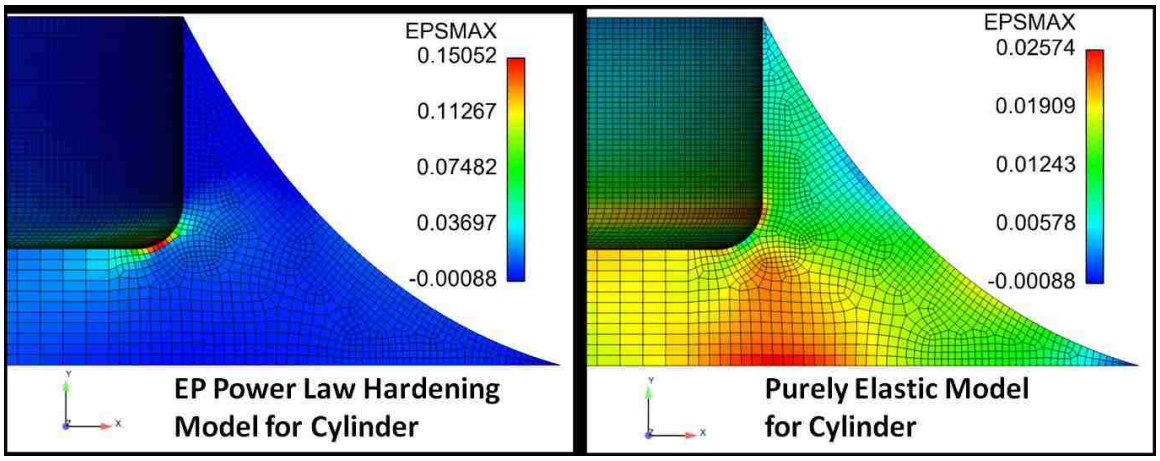

Figure 87 - Cylinder Material Model Comparison for Unfilled 828DEA at H = 0.025"

These effects of the cylinder yield zone raise additional concern about the effects of cylinder yielding on the other pusher heights. A plot of EPMAX vs. Load for all pusher heights comparing the elastic plastic power law hardening model and elastic model for the cylinder is shown in Figure 88. When examining this plot, it can be seen that the material model of the cylinder has no effect on EPSMAX predictions for pusher heights of 0.180”, 0.260” and 0.374”. This certainly demonstrates that there is a height at which the material properties contributing to the yield of the cylinder are less important in

gathering accurate failure predictions for the epoxy bond. The pusher height of 0.105" starts to show a small difference between the EPSMAX predictions of the two material models just prior to its experimental failure load of 306 lbs. At the lowest pusher height, the difference in EPSMAX predictions between the two material models deviate almost immediately after loading begins.

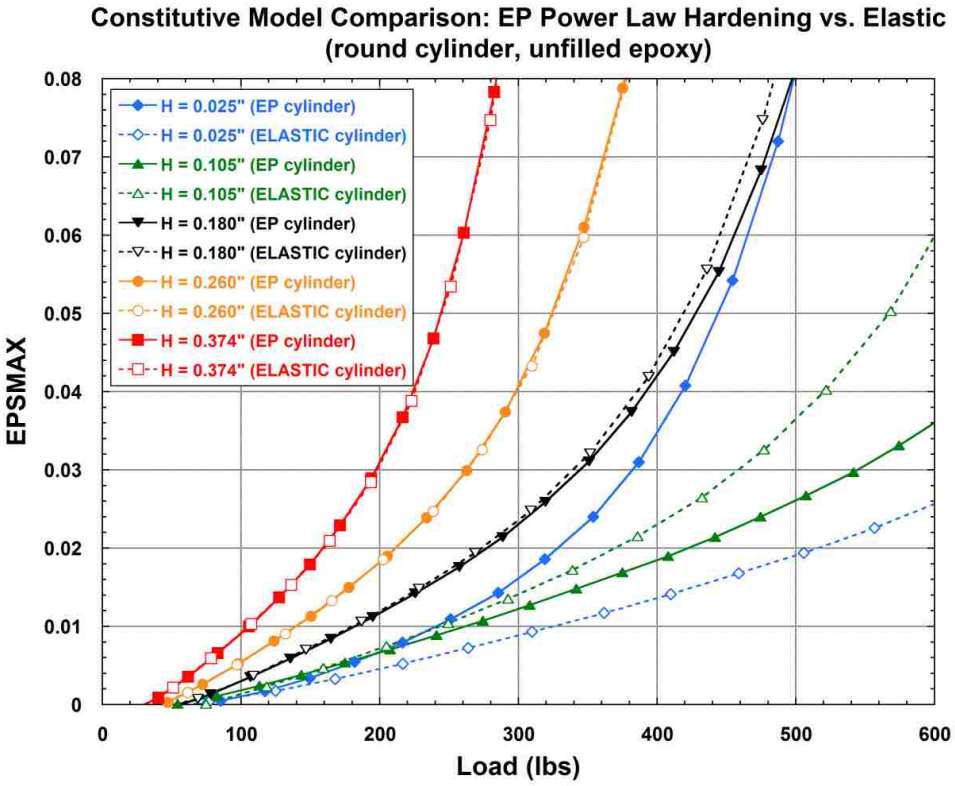

Figure 88 - EPSMAX vs. Load Comparing Cylinder Constitutive Models

The pusher height of 0.105" will also be examined because it has been shown that the material model of the cylinder seems to affect the epoxy bond predictions at that pusher height. A comparison of painted EPSMAX contour plots for the pusher height of 0.105" using the elastic plastic power law hardening model and elastic model can be seen in Figure 89.

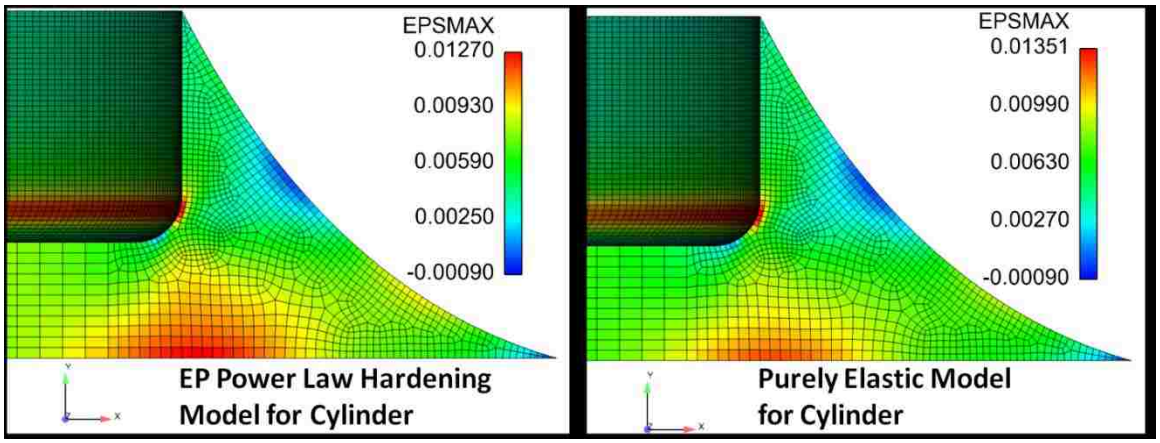

Figure 89 - Cylinder Material Model Comparison for Unfilled 828DEA at H = 0.105"

For the pusher height of 0.105" there was originally a greater EPSMAX concentration at the plate interface for unfilled 828DEA when applying the elastic plastic power law hardening model to the cylinder. When the elastic model is applied to the cylinder, the element displaying the largest value of EPSMAX is at the cylinder interface of the bond, although a secondary strain concentration is at the plate interface. The magnitude of EPSMAX is only slightly affected by the change in material model.

As done in the two geometry sensitivity studies, an additional analysis of the elastic cylinder case for the 0.260" pusher height was performed to establish an EPSMAX failure parameter. The EPSMAX failure parameter was used to determine the predicted failure load for the elastic cylinder case at pusher heights of 0.025" and 0.105". The predicted failure load for the elastic cylinder case is compared to the elastic plastic power law hardening cylinder case and experimental data in Figure 90 for the pusher height of 0.025" and in Figure 91 for the pusher height of 0.105".

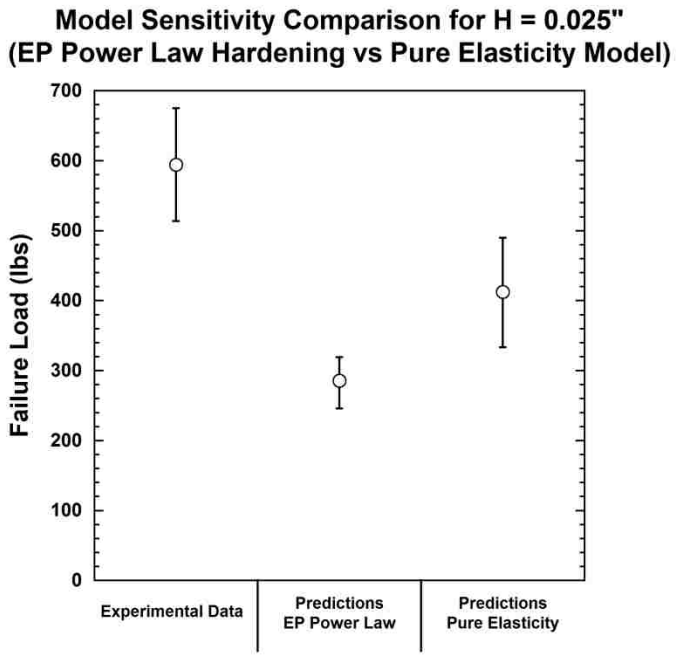

Figure 90 - Failure Load Prediction Comparing Cylinder Material Models at H = 0.025" (unfilled 828DEA)

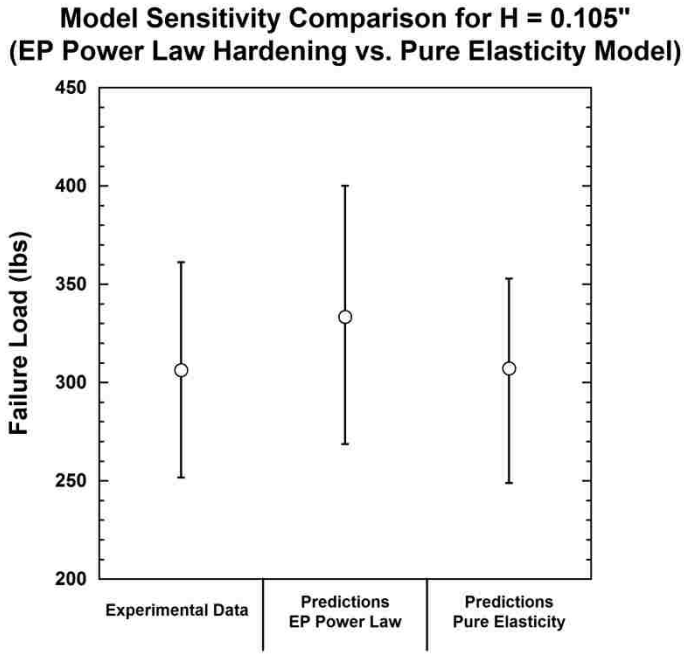

Figure 91 - Failure Load Prediction Comparing Cylinder Material Models at H = 0.105" (unfilled 828DEA)

The predicted average failure load for the pusher height of 0.025" has increased from 285 lbs using the elastic plastic power law hardening model for the cylinder, to 412 lbs when

using the pure elasticity model for the cylinder. The predicted failure load at the lowest pusher height is still lower than the experimental data. However, the nearly 45% increase in predicted failure load is now high enough that the standard deviation bounds are close to the bounds of the experimental data. Less effect is seen at the pusher height of 0.105" when using the elastic model for the cylinder. The elastic plastic power law hardening model for the cylinder matches the data well to begin with, but the slight decrease in predicted failure load when using the elastic cylinder does match better with the experimental data. The qualitative improvement of the predicted failure load for the pusher height of 0.025" implies that the cylinder may remain elastic past the point of experimental failure or that the assumed yield strength of the cylinder material may have been too low.

6.4. Failure prediction discussion

When using the elastic plastic power law hardening material model for the cylinder, the predicted failure loads for the chamfered and rounded geometries were very similar at all pusher heights for unfilled and 40vol% AlO_x 828DEA. The failure load predictions for both geometries matched the experimental data well for all pusher heights except the lowest pusher height. At the lowest pusher height, changing the thickness of the epoxy bond from 0.010" to 0.015" showed very little difference in predicted failure loads. However, changing the amount of wetting from 0.020" to 0.005" for the 0.010" thick epoxy bond showed a quantitative improvement in the magnitude of the predicted failure load and a qualitative reversal in the predicted failure load trend. In contrast, the higher pusher heights were not sensitive to geometrical variability (chamfer or round, thickness, and wetting).

The lowest pusher height sensitivities are highlighted again when changing the material model of the cylinder from elastic plastic power law hardening to pure elasticity. The compression caused by the yield zone of the cylinder interacts with the nonlinear viscoelastic response of the epoxy bond. Comparison between the two material models shows a qualitative improvement in the failure load trend when using an elastic material model for the cylinder. The higher pusher heights remain largely unaffected by the cylinder material model. With that in mind, it is possible that a combination of the elastic material model for the cylinder and smaller epoxy wetting could make the failure load prediction for the lowest pusher height match qualitatively and quantitatively within the error bounds of the data without influencing the already accurate predictions for the other pusher heights.

The predicted locus of failure changed location for the lower two pusher heights based on variations of the model geometry and material model of the cylinder. This is not necessary troublesome. If the roles were reversed and test coupons were created to exactly match the model variations, then the predicted locus of failure may in fact correspond to what is seen in those experiments.

Uncertainties in the ability to accurately model the plasticity of the metal components was the reason that load-displacement curve comparisons between the experimental data and analyses were not examined thoroughly. Although the pusher is moving at a defined displacement rate, the amount of displacement seen by the epoxy bond will be different from the pusher displacement based on the rigid body rotation of the cylinder as well as assumptions that were made regarding the rigidity of the fixture setup and the amount of plasticity in the pusher and cylinder. Regardless of those assumptions, the load recorded

by the Instron machine is still the load transferred to the epoxy bond which can be proven by a creating a simple free body diagram. A plot displaying predicted load-displacement curves based on the displacement of the pusher for all pusher heights can be seen in Appendix L. Although not necessarily representative of the displacement seen by the epoxy bond, it does show that load-displacement curves will vary based on the pusher height.

In all cases of epoxy bond geometry and cylinder material model, the load at failure does not correspond with runaway viscoelasticity on either the EPSMAX vs. Load plots or SMAX vs. EPSMAX plots. However, all cases for all pusher heights show the failure bounds occurring at a "pre-yield" of the epoxy material where the stress-strain curve begins to bend over and leave the elastic portion of the curve. A value of EPSMAX corresponding to runaway viscoelasticity may be a suitable indicator of adhesive failure initiation across all known test data, including monotonic ramp to fail and creep, but an engineer should be conscious of monotonic loadings deep in the glassy state of a polymer where the onset of yield, on a stress-strain curve, may be a more accurate and conservative indicator of adhesive failure initiation.

7. Conclusion

Experimental data follows a trend where the failure load decreases as the pusher height is increased along the length of the cylinder. Adhesive failure appeared to initiate and propagate at the cylinder interface of the epoxy bond directly below the contact region of the pusher for all samples. Modest standard deviations of 20% at some pusher heights brought into question the effect of small geometrical variability of the test coupons (bond thickness, wetting, and cylinder shape). Sensitivity studies proved that the variability contributed small amounts of error to the data, but overall did not affect the macroscopic trend of load versus pusher height for either the unfilled or 40vol% AlO_x 828DEA epoxy. For that reason, the data was believed to be of good enough quality to validate a maximum principal strain (EPSMAX) failure metric for identifying the initiation of adhesive de-bonding using the SPEC model.

Computational analyses proved to be sensitive to geometrical variability of the epoxy bond and cylinder. Simplified geometries were found inadequate, but even the accuracy of the detailed, realistic geometric model predictions were subject to mesh refinement sensitivities. For a relatively converged solution, an EPSMAX failure parameter was defined for a pusher height of 0.260" and used to accurately predict the failure of three of the other four pusher heights including 0.105", 0.180", and 0.374". The failure load prediction of the lowest pusher height did not match the load trend qualitatively or the magnitude quantitatively obtained from the data. Further geometric variability and material model changes were investigated to help explain what might be causing this discrepancy. The lowest pusher height was the only pusher location to show a significant change in predicted failure load. Qualitative and quantitative improvement was seen

when the model included a 0.005" epoxy wetting over the surface of the cylinder instead of a 0.020" value, but very few test coupons had the smaller wetting. A similar improvement was seen when using an elastic material model for the cylinder which eliminated yielding and plastic cylinder strains that were causing a compressive force on the epoxy bond. Since the higher pusher heights maintained accurate failure load predictions when using the elastic model for the cylinder, it is possible that the original assumption of the material properties for the cylinder was incorrect. The cylinders were gathered from a machine shop at Sandia Labs and there may have been some sort of heat treatment or other change to the stainless steel cylinders that raised the yield strength in a way not accounted for in the analyses. Analyses clearly showed that less yielding in the cylinder produces more accurate failure load predictions.

Possible uncertainties in the material properties for the cylinder and epoxy bond geometry are reason enough to potentially disregard the analyses at that pusher height. Fortunately, the other four pusher locations are far enough away from the epoxy bond that inaccurate assumptions in the geometry or material model of the cylinder do not affect failure predictions. Analyses of these pusher heights capture accurate failure load predictions for unfilled and 40vol% AlO_x 828DEA epoxy. Additionally, predicted failure loads for all pusher heights seem to correlate to a pre-yield of the epoxy material on a stress-strain curve (close to the onset of nonlinearity). Pre-yield of the epoxy could be a suitable conservative indicator of failure initiation when an EPSMAX failure parameter has not been established. The SPEC model has previously been used to develop an adhesive failure initiation parameter using EPSMAX as an indicator of runaway viscoelasticity for failure predictions of simple napkin ring test geometries undergoing

one mode of loading. Experiments in this study had complex geometrical features undergoing mixed modes of loading and high strain gradients, but the SPEC model was still able to be used to predict the initiation of de-bonding consistently. Experiments and analyses of the test coupon presented in this thesis continue to show the usefulness of EPSMAX near runaway viscoelasticity as a viable predictor of adhesive failure initiation in glassy thermosets such as epoxies.

APPENDICES

APPENDIX A Experimental Data for H = 0.025" (unfilled)

Batch 1 (03/24/2011)		
Sample #	Bond Thickness (in)	Failure Load (lbs)
1	0.015	620.63
2	0.015	604.34
3	0.012	676.46
4	0.013	522.76
5	0.01	681.38
6	0.008	626
7	0.013	727.21
8	0.014	706.47
9	0.01	680.21
10	0.018	608.74

Batch 2 (03/30/2011)		
Sample #	Bond Thickness (in)	Failure Load (lbs)
1	0.013	525.36
2	0.013	510.31
3	0.014	597.02
4	0.014	468.54
5	0.013	569.89
6	0.01	527.81
7	0.013	515.29
8	0.016	623.3
9	0.015	666.82
10	0.012	463.98

Batch 3 (04/14/2011)		
Sample #	Bond Thickness (in)	Failure Load (lbs)
1	0.014	621.26
2	0.012	541.08
3	0.014	531.13
4	0.012	587.29
5	0.009	429.69
6	0.013	688.45
7	0.011	692.85
8	0.009	620.51

APPENDIX B Experimental Data for H = 0.025" (40vol% AlO_x)

Batch 1 (08/01/2011)		
Sample #	Bond Thickness (in)	Failure Load (lbs)
1	0.012	581.53
2	0.012	545.65
3	0.013	613.05
4	0.014	604.29
5	0.009	638.36
6	0.01	521.18
7	0.014	595.96
8	0.01	590.22
9	0.012	495.04

Batch 2 (08/08/2011)		
Sample #	Bond Thickness (in)	Failure Load (lbs)
1	0.012	436.46
2	0.011	618.78
3	0.013	645.34
4	0.012	566.59
5	0.012	542.38
6	0.012	498.55
7	0.012	519.6
8	0.013	605.84
9	0.012	548.13
10	0.012	523.13

Batch 3 (08/15/2011)		
Sample #	Bond Thickness (in)	Failure Load (lbs)
1	8/15/2011 Tests (H = 25mil) 40% AlOx	
2	0.013	505.18
3	0.011	562.32
4	0.013	571.33
5	0.011	559.18
6	0.013	529.16
7	0.013	457.7
8	0.014	505.84
9	0.012	534.9

APPENDIX C Experimental Data for H = 0.105" (Unfilled)

Batch 1 (04/28/2011)		
Sample #	Bond Thickness (in)	Failure Load (lbs)
1	0.015	284.44
2	0.010	327.17
3	0.012	356.01
4	0.013	352.46
5	0.014	241.39
6	0.012	214.92
7	0.013	388.41
8	0.014	262.37
9	0.015	341.84
10	0.014	226.72

Batch 2 (05/09/2011)		
Sample #	Bond Thickness (in)	Failure Load (lbs)
1	0.010	391.65
2	0.012	313.62
3	0.009	332.52
4	0.013	374.45
5	0.010	318.87
6	0.014	335.71
7	0.011	262.62
8	0.012	326.65
9	0.011	323.51
10	0.013	313.22

Batch 3 (05/11/2011)		
Sample #	Bond Thickness (in)	Failure Load (lbs)
1	0.012	302.14
2	0.012	192.33
3	0.013	263.51
4	0.014	200.4
5	0.012	353.79
6	0.013	292.29
7	0.011	336.48
8	0.013	365.39
9	0.011	288.08

APPENDIX D Experimental Data for H = 0.105" (40vol% AlO_x)

Batch 1 (07/25/2011)		
Sample #	Bond Thickness (in)	Failure Load (lbs)
1	0.013	384.70
2	0.013	334.20
3	0.013	263.45
4	0.015	422.33
5	0.017	338.77
6	0.011	340.70
7	0.012	391.12
8	0.014	310.20
9	0.012	370.62

Batch 2 (07/25/2011)		
Sample #	Bond Thickness (in)	Failure Load (lbs)
1	0.017	349.01
2	0.015	381.06
3	0.016	325.74
4	0.012	357.63
5	0.012	300.81
6	0.014	340.34
7	0.014	379.56
8	0.013	340.00
9	0.010	374.74

APPENDIX E Experimental Data for H = 0.180" (Unfilled)

Batch 1 (09/16/2011)		
Sample #	Bond Thickness (in)	Failure Load (lbs)
1	0.011	191.98
2	0.012	248.37
3	0.012	235.62
4	0.010	246.91
5	0.011	246.17
6	0.011	279.35
7	0.013	263.79
8	0.012	215.79
9	0.016	238.24

Batch 2 (09/21/2011)		
Sample #	Bond Thickness (in)	Failure Load (lbs)
1	0.011	319.54
2	0.010	278.61
3	0.011	252.74
4	0.012	245.16
5	0.011	225.32
6	0.012	294.55
7	0.010	358.63
8	0.012	360.08
9	0.012	292.98
10	0.011	305.85

APPENDIX F Experimental Data for H = 0.180" (40vol% AlO_x)

Batch 1 (09/16/2011)		
Sample #	Bond Thickness (in)	Failure Load (lbs)
1	0.010	321.06
2	0.012	270.67
3	0.015	257.49
4	0.011	302.56
5	0.012	307.35
6	0.016	258.44
7	0.016	221.29
8	0.015	313.74

APPENDIX G Experimental Data for H = 0.260" (Unfilled)

Batch 1 (05/13/2011)		
Sample #	Bond Thickness (in)	Failure Load (lbs)
1	0.011	158.93
2	0.014	206.75
3	0.010	161.71
4	0.013	220.26
5	0.012	165.1

Batch 2 (05/17/2011)		
Sample #	Bond Thickness (in)	Failure Load (lbs)
1	0.012	179.81
2	0.015	163.46

Batch 3 (05/19/2011)		
Sample #	Bond Thickness (in)	Failure Load (lbs)
1	0.013	205.32
2	0.012	111.94
3	0.014	144.83
4	0.011	151.88
5	0.016	161.56
6	0.010	226.49
7	0.013	177.65
8	0.012	151.78
9	0.016	173.03

APPENDIX H Experimental Data for H = 0.260" (40vol% AlO_x)

Batch 1 (06/20/2011)		
Sample #	Bond Thickness (in)	Failure Load (lbs)
1	0.014	259.78
2	0.013	242.21
3	0.011	206.57
4	0.014	232.71
5	0.012	260.96
6	0.014	228.41
7	0.013	272.86
8	0.014	214.97
9	0.007	271.31
10	0.014	234.34

Batch 2 (07/01/2011)		
Sample #	Bond Thickness (in)	Failure Load (lbs)
1	0.014	195.73
2	0.014	212.71
3	0.014	188.48
4	0.013	186.46
5	0.016	199.66
6	0.014	152.17
7	0.014	210.79
8	0.011	206.78
9	0.013	151.98

Batch 3 (07/18/2011)		
Sample #	Bond Thickness (in)	Failure Load (lbs)
1	0.012	167.73
2	0.014	175.46
3	0.015	150.97
4	0.018	172.62
5	0.016	180.87
6	0.013	145.37
7	0.009	219.97
8	0.011	185.50
9	0.013	175.69
10	0.014	154.90

APPENDIX I Experimental Data for H = 0.374" (Unfilled)

Batch 1 (06/20/2011)		
Sample #	Bond Thickness (in)	Failure Load (lbs)
1	0.013	92.83
2	0.012	142.44
3	0.013	133.56
4	0.013	129.45
5	0.014	101.14
6	0.012	125.91
7	0.013	118
8	0.015	114.28
9	0.014	109.6

Batch 2 (06/23/2011)		
Sample #	Bond Thickness (in)	Failure Load (lbs)
1	0.010	164.78
2	0.012	141.90
3	0.013	141.94
4	0.013	166.82
5	0.014	152.05
6	0.011	151.34
7	0.011	139.06
8	0.012	143.94
9	0.012	144.36
10	0.012	144.97

Batch 3 (08/29/2011)		
Sample #	Bond Thickness (in)	Failure Load (lbs)
1	0.012	138.81
2	0.012	122.12
3	0.011	128.96
4	0.011	117.80
5	0.010	126.33
6	0.010	125.71
7	0.012	127.07

APPENDIX J Experimental Data for H = 0.374" (40vol% AlO_x)

Batch 1 (07/11/2011)		
Sample #	Bond Thickness (in)	Failure Load (lbs)
1	0.014	153.52
2	0.015	126.96
3	0.016	141.03
4	0.013	170.39
5	0.014	124.38
6	0.016	167.61
7	0.012	173.76
8	0.016	172.54
9	0.013	154.84
10	0.013	135.77

Batch 2 (07/11/2011)		
Sample #	Bond Thickness (in)	Failure Load (lbs)
1	0.012	119.21
2	0.011	96.96
3	0.01	163.93
4	0.01	133.35
5	0.01	135.1
6	0.013	148.92
7	0.014	138.27
8	0.014	141.63
9	0.015	116.34

Batch 3 (07/15/2011)		
Sample #	Bond Thickness (in)	Failure Load (lbs)
1	0.011	176.08
2	0.012	170.49
3	0.01	182.23
4	0.01	170.05
5	0.011	190.15
6	0.016	193.08
7	0.013	181.42
8	0.014	172.67
9	0.015	199.51
10	0.011	180.92

APPENDIX K Average Experimental Data Values

Pusher Height 0.025" (Unfilled)				
Batch	**Avg. Bond Thickness (in)**	**Bond Thickness Std. Dev. (in)**	**Avg. Load at Failure (lbs)**	**Load at Failure Std. Dev. (lbs)**
1	0.013	0.003	645.42	60.51
2	0.013	0.002	546.83	66.20
3	0.012	0.002	589.03	87.62
AVG:	**0.013**	**0.002**	**594.10**	**80.51**

Pusher Height 0.025" (40vol% AlOx)				
Batch	**Avg. Bond Thickness (in)**	**Bond Thickness Std. Dev. (in)**	**Avg. Load at Failure (lbs)**	**Load at Failure Std. Dev. (lbs)**
1	0.012	0.002	576.14	46.33
2	0.012	0.001	550.48	61.88
3	0.012	0.001	531.71	36.94
AVG:	**0.012**	**0.001**	**552.70**	**51.46**

Pusher Height 0.105" (Unfilled)				
Batch	**Avg. Bond Thickness (in)**	**Bond Thickness Std. Dev. (in)**	**Avg. Load at Failure (lbs)**	**Load at Failure Std. Dev. (lbs)**
1	0.013	0.002	299.57	61.37
2	0.012	0.002	329.28	35.08
3	0.012	0.002	288.27	61.55
AVG:	**0.012**	**0.002**	**306.31**	**54.75**

Pusher Height 0.105" (40vol% AlOx)				
Batch	**Avg. Bond Thickness (in)**	**Bond Thickness Std. Dev. (in)**	**Avg. Load at Failure (lbs)**	**Load at Failure Std. Dev. (lbs)**
1	0.013	0.002	350.68	47.55
2	0.014	0.002	349.88	26.72
AVG:	**0.014**	**0.002**	**351.01**	**37.42**

APPENDIX K (continued) Average Experimental Data Values

Pusher Height 0.180" (Unfilled)				
Batch	**Avg. Bond Thickness (in)**	**Bond Thickness Std. Dev. (in)**	**Avg. Load at Failure (lbs)**	**Load at Failure Std. Dev. (lbs)**
1	0.012	0.002	240.69	25.45
2	0.011	0.001	293.35	45.18
AVG:	**0.012**	**0.001**	**268.40**	**45.15**

Pusher Height 0.180" (40vol% AlOx)				
Batch	**Avg. Bond Thickness (in)**	**Bond Thickness Std. Dev. (in)**	**Avg. Load at Failure (lbs)**	**Load at Failure Std. Dev. (lbs)**
1	0.013	0.002	281.58	34.98
AVG:	**0.013**	**0.002**	**281.58**	**34.98**

Pusher Height 0.260" (Unfilled)				
Batch	**Avg. Bond Thickness (in)**	**Bond Thickness Std. Dev. (in)**	**Avg. Load at Failure (lbs)**	**Load at Failure Std. Dev. (lbs)**
1	0.012	0.002	182.55	28.74
2	0.014	0.002	171.64	11.56
3	0.013	0.002	167.16	33.86
AVG:	**0.013**	**0.002**	**172.53**	**29.86**

Pusher Height 0.26" (40vol% AlOx)				
Batch	**Avg. Bond Thickness (in)**	**Bond Thickness Std. Dev. (in)**	**Avg. Load at Failure (lbs)**	**Load at Failure Std. Dev. (lbs)**
1	0.013	0.002	242.41	23.10
2	0.014	0.001	189.42	23.03
3	0.014	0.003	172.91	21.19
AVG:	**0.013**	**0.002**	**202.00**	**37.47**

Pusher Height 0.374"(Unfilled)				
Batch	**Avg. Bond Thickness (in)**	**Bond Thickness Std. Dev. (in)**	**Avg. Load at Failure (lbs)**	**Load at Failure Std. Dev. (lbs)**
1	0.013	0.001	118.58	15.94
2	0.012	0.001	149.12	9.68
3	0.011	0.001	126.69	6.50
AVG:	**0.012**	**0.001**	**132.51**	**17.74**

APPENDIX K (continued) Average Experimental Data Values

Pusher Height 0.374" (40vol% AlOx)				
Batch	**Avg. Bond Thickness (in)**	**Bond Thickness Std. Dev. (in)**	**Avg. Load at Failure (lbs)**	**Load at Failure Std. Dev. (lbs)**
1	0.014	0.001	152.08	19.04
2	0.012	0.002	132.63	19.63
AVG:	**0.013**	**0.002**	**142.87**	**21.26**

APPENDIX L Predicted Load vs. Displacement Plot

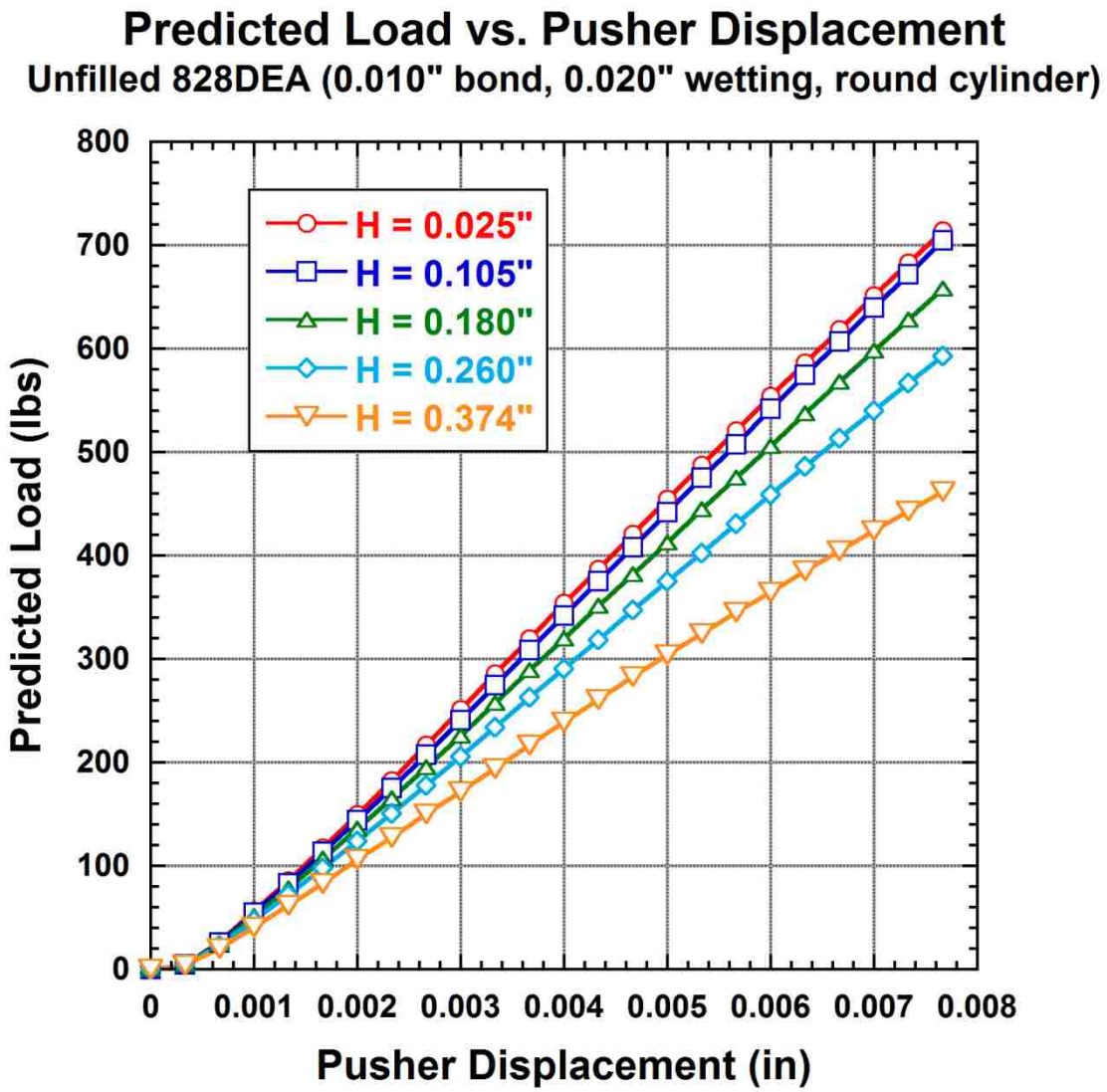

References

[1] James M. Caruthers, Douglas B. Adolf, Robert S. Chambers, Prashant Shrikhande (2004) 'A thermodynamically consistent, nonlinear viscoelastic approach for modeling glassy polymers', Polymer, 45: 4577-4597

[2] Douglas B. Adolf, Robert S. Chambers, James M. Caruthers (2004) 'Extensive validation of a thermodynamically consistent, nonlinear viscoelastic model for glassy polymers, Polymer, 45: 4599-4621

[3] Adolf, Douglas B. , Chambers, Robert S. , Neidigk, Matthew A. (2009) 'A simplified potential energy clock model for glassy polymers', Polymer, 50: 4257-4269

[4] Adolf, Doug , Spangler, Scott , Austin, Kevin , Neidigk, Matthew , Neilsen, Mike , Chambers, Robert (2011) 'Packaging Stratagies for Printed Circuit Board Components Volume 1: Materials & Thermal Stresses', Prepared by Sandia National Laboratories: Sandia Report SAND2011-4751 (Unlimited Release)

[5] Adolf, Douglas B. , Chambers, Robert S. , Elisberg, Brenton , Ruff, Mary , Stavig, Mark (2010) 'Predicting Cohesive Failure in Thermosets', The Journal of Applied Polymer Science, 119: 4, 2143-2152

[6] Adolf, Douglas B. , Chambers, Robert S. , Hance, Brad and Elisberg, Brenton (2010) 'Predicting the Initiation of Thermoset De-Bonding', The Journal of Adhesion, 86: 11, 1111-1131

[7] Neidigk, Matthew A., Shen, Yu-Lin , 'Effect of Underfill Filler Volume Fraction on Solder Fatigue Life for Surface Mount Components Using Nonlinear Viscoelastic Finite Element Analyses', not yet published

[8] ADAGIO/ANDANTE Users Reference Manual, Sandia National Laboratories, Albuquerque, New Mexico, 2005

[9] Stone, Charles M. , Wellman, Gerald W. , Krieg, Raymond D. , (1990) 'A Vectorized Elastic / Plastic Power Law Hardening Model Including Lüders Strain', Prepared by Sandia National Laboratories: Sandia Report SAND09-0153 (Unlimited Release)